Winter January 6, 2014

Sterically Engineered Perylene Dyes for High Efficiency Oriented Fluorophore Luminescent Solar Concentrators

Stephen R. McDowall, *Western Washington University*
Willie E. Benjamin, *Western Washington University*
Darren R. Veit, *Western Washington University*
Matt J. Perkins, *Western Washington University*
Edward Bain, *Western Washington University*, et al.

CHEMISTRY OF MATERIALS

Communication

pubs.acs.org/cm

Sterically Engineered Perylene Dyes for High Efficiency Oriented Fluorophore Luminescent Solar Concentrators

Willie E. Benjamin,[†] Darren R. Veit,[†] Matt J. Perkins,[†] Edward Bain,[†] Kelsey Scharnhorst,[†] Stephen McDowall,[‡] David L. Patrick,*[,†] and John D. Gilbertson*[,†]

[†]Department of Chemistry and [‡]Department of Mathematics, Western Washington University, Bellingham, Washington 98225, United States

Supporting Information

Luminescent solar concentrators (LSCs) collect and concentrate sunlight for use in solar power generation.[1] First proposed over 30 years ago,[1d] LSCs are simple devices, consisting of a planar waveguide coated or impregnated with a fluorophore. The fluorophore absorbs sunlight, re-emitting it into the waveguide where it travels to a device edge for conversion by photovoltaic (PV) cells. LSCs have attracted attention due to their high theoretical concentration factors, their ability to provide wavelength-to-bandgap matched photons, and because they function equally well under diffuse and direct illumination.[2] Unlike other concentrator designs, LSCs selectively harvest light in a particular spectral band (determined by the absorption range of the fluorophore) allowing other wavelengths to pass through for secondary applications such as thermal generation or interior lighting, increasing the combined-cycle efficiency. Accordingly, LSC performance is expressed in terms of the optical quantum efficiency (OQE), defined as the fraction of absorbed photons concentrated at the edge. Despite several decades of research, LSC OQEs remain too low for most practical applications and decrease rapidly with LSC size. For dyes possessing high fluorescent quantum yield (FQY), light trapping efficiency is limited primarily by waveguide escape cone (EC) losses defined by Snell's Law.[3] An approach to circumvent such losses involves orientation of the dye's emission transition moment perpendicular to the plane of the concentrator, which leads to preferential emission into guided modes.[4] Ballistic photon Monte Carlo simulations predict alignment that can reduce EC losses from about 25% to under 10% *per emission* in an air-clad waveguide with a refractive index of 1.5, depending on the degree of orientational order.[3] Since EC losses compound due to repetitive reabsorption and re-emission caused by overlap of fluorophore absorption and emission spectra, fluorophore alignment, combined with reduced self-absorption,[5] has the potential to significantly improve LSC efficiency. Here, we focus on the former approach.

Previous attempts to prepare oriented fluorophore LSCs demonstrated modest performance gains, limited by the degree of fluorophore orientational order, solubility, or FQY.[4b,6] Here we report a new family of perylenebisimide (PBI) dyes designed for oriented fluorophore LSCs which address these limitations. Incorporation into optically transparent polymerizable liquid crystal (LC) waveguides results in devices with OQE = 74% at a geometric gain $G = 10$, where G is the ratio of facial to perimeter area.

We studied a series of PBIs of the type *N*,*N*-bis(2,6-diisopropyl-4-octylaniline)-perylene-3,4,9,10-tetracarboximide, containing pendant orthoalkylated anilines with long alkyl tails (Chart 1). The PBI luminophore is widely used for LSC applications[7a] because it confers intense absorbance, good photostability, and near unity quantum yield; however, $\pi-\pi$ stacking in unsubstituted PBIs severely limits their solubility.[7b] Addition of bulky pendant aromatic groups orthoalkylated at aniline positions 2 and 6 (e.g., compound **8**, Chart 1) improves solubility in organic solvents;[7] however, the concomitant reduction in molecular aspect ratio causes poor alignment in LC guest–host systems (the scalar orientational order parameter of the absorption transition moment[8] of **8** in the nematic LC 4′-pentyl-4-cyanobiphenyl (5CB) is $s = 0.22$, Table 1, see also the Supporting Information).[9] Addition of long alkyl tails (compound **7**) to increase the aspect ratio raises s only

Chart 1. Abbreviated Molecular Structure(s) of the Full Series of Flourophores Synthesized for This Study and the Complete Molecular Structures of 3 and 4[a]

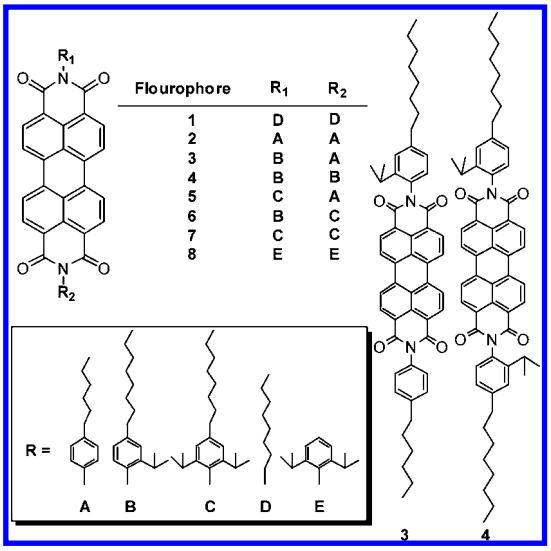

[a]It should be noted that **4** is likely a mixture of *syn*- and *anti*- isomers.

Received: October 6, 2013
Revised: January 5, 2014
Published: January 6, 2014

Table 1. Summary of Fluorophore Properties

fluorophore	solubility[a]	s^b	FQY[c]	sterics[d]
1	0.13	0.62	0.95	{0,0}
2	0.15	0.68	0.98	{0,0}
3	4.9	0.68	0.92	{1,0}
4	1.1	0.65	0.96	{1,1}
5	7.3	0.53	0.92	{2,0}
6	22	0.62	0.98	{1,2}
7	0.45	0.32	0.98	{2,2}
8	0.14	0.22	0.99	{2,2}

[a]Solubility in 5CB (mg/mL). [b]s is the scalar order parameter for the absorption transition moment. [c]Measured in $CHCl_3$ at 25 °C. [d]Sterics are defined as the number of orthoisopropyl groups on the pendant imide on each side of the PBI molecule.

slightly, to 0.29, insufficient for LSC applications. If the orthoisopropyl groups are removed (compound **2**), s increases sharply, to 0.68, but the solubility is again low. Hence there exists a trade-off in the use of bulky substituents with respect to solubility and alignability, a challenge commonly encountered in guest−host LC systems.[10a] To understand this result we note that, in the absence of directional chemical interactions such as H-bonding, general alignment trends in nematic LC hosts are largely determined by the geometry of the guest's excluded volume, v against rod-shaped nematogens, which for optimal alignment should be such that v is minimized when guest molecules orient parallel to the LC director.[10] A geometry v which disrupts local nematic order also affects solubility, since the free energy density of the LC host is coupled to its order parameter.[11] At the same time, for the dyes studied here, an additional solubility prerequisite is that PBI−PBI $\pi-\pi$ stacking should be inhibited, preventing aggregate formation.[12] This suggests the optimal steric design for achieving both high solubility and alignment is a molecular architecture permitting close colinear approach between nematogens and the PBI core but preventing it for pairs of dye molecules.

To achieve this, we studied the effect of asymmetric steric substitution at the aniline in the family of compounds shown in Chart 1. The full compilation of fluorophores synthesized in this study (See Supporting Information for details) and their properties are listed in Table 1. Fluorophores **1** and **8** are commercially available. As expected,[7b] their optical properties ($\lambda_{abs,max}$, $\lambda_{em,max}$, ε, and Φ_f) are virtually identical (Table 1 and Table S1 in the SI), though their solubilities and orientational order parameters in 5CB vary widely. Focusing on the latter, we observe that increasing the number of orthoisopropyl groups $\{m,n\}$ from {0,0} in **1** and **2** (where m and n are the number of orthoisopropyl groups on the first and second imides, respectively) to {1,2} in **6** results in a steady, significant increase in solubility (from ∼0.1 to 22 mg/mL) as $m + n$ increases from 0 to 3, and uniformly high order parameters. Strikingly though, addition of a fourth orthoisopropyl group in **7** to produce the {2,2} configuration results in a large decrease in both the order parameter and solubility. The values are similar to those obtained for **8** (no alignable tails). The data in Table 1 also show that addition of alkyl chains to the para position of the pendant imide results in an increase in orientational order, consistent with previous studies showing that extension of the long axis leads to higher order parameters up to a chain length of eight carbons, after which longer chains are detrimental to alignment and solubility.[13]

The above results are consisent with a model in which asymmetric subsitution (about the long molecular axis of the guest) permits favorable colinear nematogen−PBI core interactions up to $m + n \leq 3$ but inhibits the same for pairs of PBI cores with $m + n > 1$ (Figure 1). Combined with long alkyl tails to increase the molecular aspect ratio, the asymmetric fluorophores **3**−**6** having the configurations {1,0}, {1,1}, {2,0}, and {2,1} are both highly soluble and highly oriented.

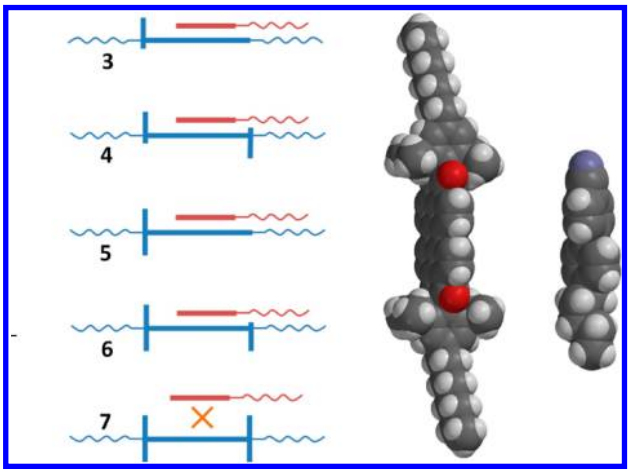

Figure 1. Schematic illustration (left) of the effect of steric placement on nematogen (red)−PBI (blue) colinear interactions in **3**−**7**. Space filling model (right) demonstrating the restricted mesogen access to the perylene core of **7**.

We demonstrate the effect of dye orientation on LSC performance in a device based on a representative member of this group (**4**) incorporated into the photopolymerizable LC RMM28A (Merck). **4** was selected due to its intermediate solubility, alignability, and relative synthetic ease (compared to fluorophores **3**, **5**, and **6**).[14] LSCs were fabricated as 1−5 μm thick films spin-cast onto borosilicate glass coverslips, photopolymerized to produce uniform homeotropic alignment to the plane of the film. The order parameter for the absorption transition moment of **4** was measured to be s = 0.77 in the photopolymerized matrix, somewhat higher than in 5CB.[15] LSCs were uniformly illuminated with 485 nm monochromatic light and emission from an aperture of length l = 0.7 cm centered on one edge was collected by an integrating sphere coupled to a fluorometer. The remaining device edges were blackened. Samples measured 2.5 × 2.5 × 0.16 cm, resulting in a geometric gain G = 10. Facial absorption and edge emission spectra for a representative device are shown in Figure 2. Experimental details are presented in the Supporting Information.

After correcting for the aperture size and edge-escape cone angle (see Supporting Information for discussion), we find OQE = 74%, the highest efficiency observed so far in a LSC device and significantly exceeding the previous highest reported OQE of ∼50%.[16] The results are in good agreement with predictions from ballistic Monte Carlo simulations (predicted OQE = 70%) performed using a model based on the experimentally measured absorption and emission spectra, film refractive indices, dye order parameter, FQY, and device absorbance and dimensions.[15] For comparison, the limiting upper theoretical OQE for an LSC incorporating fluorophores with an order parameter s = 0.8 is approximately 84%, assuming unity FQY, a single escape cone loss, and a waveguide refractive

dx.doi.org/10.1021/cm403286v | Chem. Mater. 2014, 26, 1291−1293

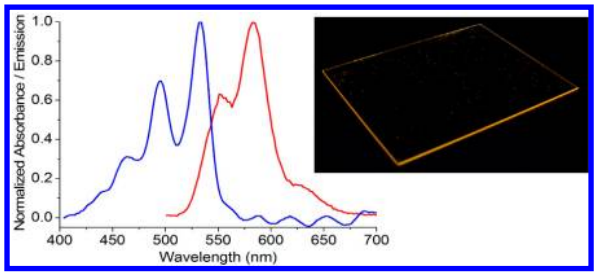

Figure 2. Normalized absorption (blue) and emission (red) spectra of **4** in photopolymerized RMM28A. Inset: photograph of an LSC device imaged under UV illumination.

index of 1.5.[3] The somewhat lower efficiency observed here can be accounted for by self-absorption resulting from the small Stokes shift, which leads to repeated escape cone losses as well as nonunity FQY. Although devices were prepared using a relatively low dye concentration (1000 ppm) to isolate the effects of alignment, attenuation of the highest energy vibronic peak in the emission spectrum shown in Figure 2 (relative to the intensity of the second and third transitions) indicates some self-absorption in these devices.[17]

In summary, a systematic analysis of the effects of molecular structure on solubility and guest–nematic host alignment in a series of perylenebisimide fluorophores was undertaken, and a model is proposed for optimal steric architecture based on asymmetric pendant anilines having long alkyl tails. Incorporation of one such fluorophore into a LSC device with homeotropic alignment resulted an optical quantum efficiency of 74%, the highest reported to date. Further efficiency improvements may be possible through the use of oriented fluorophores having larger Stoke's shifts and higher FQY. Finally, we note that the steric design principles articulated here should be applicable to a wide range of other guest–nematic host systems, including guest–host LC displays.

■ ASSOCIATED CONTENT

Ⓢ Supporting Information

Experimental details, *s* determination, selected spectra, device fabrication, and description of mathematical model. This material is available free of charge via the Internet at http://pubs.acs.org.

■ AUTHOR INFORMATION

Corresponding Authors

*E-mail: david.patrick@wwu.edu.
*E-mail: gilbertson@chem.wwu.edu.

Notes

The authors declare no competing financial interest.

■ ACKNOWLEDGMENTS

This work was supported by the National Science Foundation (NSF) Grant DMR-1035512 and an award from WWU AMSEC.

■ REFERENCES

(1) (a) Batchelder, J. S.; Zewail, A. H.; Cole, T. *Appl. Opt.* **1981**, *20*, 3733. (b) Batchelder, J. S.; Zewail, A. H.; Cole, T. *Appl. Opt.* **1981**, *18*, 3090. (c) Debije, M. G.; Verbunt, P. C. *Adv. Energy Mater.* **2012**, *2*, 12–35. (d) Weber, W. H.; Lambe, J. *Appl. Opt.* **1976**, *15*, 2299.

(2) (a) Smestad, G.; Ries, H.; Winston, R.; Yablonovitch, E. *Sol. Energy Mater.* **1990**, *21*, 99. (b) Goetzberger, A.; Wittwer, V. *Sol. Cells* **1981**, *4*, 3.

(3) McDowall, S.; Butler, T.; Bain, E.; Scharnhorst, K.; Patrick, D. L. *Appl. Opt.* **2013**, *52*, 1230.

(4) (a) McDowall, S.; Johnson, B. L.; Patrick, D. L. *J. Appl. Phys.* **2010**, *108*, 053508. (b) Debije, M. G.; Broer, D. J.; Bastiaansen, C. W. M. Presented at the 22nd European Photovoltaic Solar Energy Conference, Milan, Italy, 3–7 September 2007. (c) Mulder, C. L.; Reusswig, P. D.; Velázquez, A. M.; Kim, H.; Rotschild, C.; Baldo, M. A. *Opt. Expr.* **2010**, *18*, A79. (d) MacQueen, R. W.; Cheng, Y. Y.; Clady, R. G. C. R.; Schmidt, T. W. *Opt. Expr.* **2010**, *18*, A161.

(5) Krumer, Z.; van Sark, W. G. J. H. M.; Donega, C.; de, M.; Schropp, R. E. I. *Proc. SPIE* **2013**, *8821*, 882104.

(6) (a) Debije, M. G. *Adv. Funct. Mater.* **2010**, *20*, 1498. (b) Kaiser, A.; Hermans, K.; Bastiaansen, C. W. M.; Broer, D. J.; Debije, M. G. *Adv. Funct. Mater.* **2009**, *19*, 2714.

(7) (a) Seybold, G.; Wagenblast, G. *Dyes Pigm.* **1989**, *11*, 303. (b) Würthner, F. *Chem. Comm* **2004**, 1564. (c) Deyama, K.; Tomoda, H.; Murumatsu, H.; Matsui, M. *Dyes Pigm.* **1996**, *30*, 73. (d) Langhals, H.; Ismael, R.; Yürük, O. *Tetrahedron* **2000**, *56*, 5435. (e) Frischmann, P. D.; Würthner, F. *Org. Lett.* **2013**, *15*, 4674.

(8) The 0 → 1 absorption transition moment is parallel to the long PBI axis. See Johansson, L. B. A.; Langhals, H. *Spectrochim. Acta* **1991**, *47A*, 857.

(9) Fritz, K. P.; Scholes, G. D. *J. Phys. Chem. B* **2003**, *107*, 10141.

(10) (a) Cox, R. J. *Mol. Cryst. Liq. Cryst.* **1979**, *55*, 1. (b) Onsager, L. *Ann. N.Y. Acad. Sci.* **1949**, *51*, 627. (c) Frenkel, D.; Polson, J. M. *Phys. Rev. E.* **1997**, *56*, 6260.

(11) *The Physics of Liquid Crystals*, 2nd ed.; de Gennes, P. G., Prost, J., Eds.; Clarendon Press: Oxford, 1993.

(12) Donati, F.; Pucci, A.; Cappelli, C.; Mennucci, B.; Ruggeri, G. *J. Phys. Chem. B* **2008**, *112*, 3668.

(13) Leslie, T. M.; Goodby, J. W.; Filas, R. W. *Liq. Cryst. Ordered Fluids* **1984**, *4*, 43.

(14) It should be noted that **4** may be a mixture of the *syn*- and *anti*-isomers. Only one product was separable via chromatography and temperature-dependent NMR indicated only a single product was present.

(15) See Supporting Information.

(16) Currie, M. J.; Mapel, J. K.; Heidel, T. D.; Goffri, S.; Baldo, M. A. *Science* **2008**, *321*, 226.

(17) Sansregret, J.; Drake, J. M.; Thomas, W. R. L.; Lesiecki, M. L. *Appl. Opt.* **1983**, *22*, 573.

Sterically Engineered Perylene Dyes for High Efficiency Oriented Fluorophore Luminescent Solar Concentrators

Willie E. Benjamin,[a] Darren R. Veit,[a] Matt J. Perkins,[a] Edward Bain,[a] Kelsey Scharnhorst,[a] Stephen McDowall,[b] David L. Patrick,*[a] and John D. Gilbertson*[a]

[a] *Department of Chemistry, Western Washington University, Bellingham, WA, 98225, USA*
[b] *Department of Mathematics, Western Washington University, Bellingham, WA, 98225, USA*

Table of Contents

General Procedures

All reactions were carried out under dry nitrogen atmosphere using standard Schlenk-line technique unless otherwise noted. Perylene-3,4,9,10-tetracarboxylic dianhydride (97%), bis(triphenylphosphine)palladium(II) dichloride (≥99%), palladium on carbon (10 wt. % loading), imidazole (≥99%), and iodine (≥99.8%) were purchased from Aldrich and used without further purification. 4-hexylaniline (90%), 2,6-diisopropylaniline (90%), and 2-isopropylaniline (97%) were purchased from Aldrich and purified via distillation over sodium hydroxide. Potassium carbonate, anhydrous, granular (99.0% min.), and p-toluenesulfonic acid monohydrate (99.0% min.) were purchased from J.T. Baker and used without further purification. 1-octyne (98%) was purchased from Alfa Aesar and used without further purification. Hydrogen gas (99.999%) was purchased from Praxair Distribution, Inc. Column chromatography was performed on silica gel (mesh size 50-63 μm). Chromatography solvents dichloromethane (≥99.5%), chloroform (≥99.8%), hexanes (≥98.5%), ethyl acetate (≥99.9%), and acetone (≥99.5%) were purchased from Macron and used without further purification. Diethyl ether, anhydrous (≥99.9%) was purchased from J.T. Baker and used without further purification. All other solvents were dried and deoxygenated using a PureSolv solvent purification system (CuO and alumina columns). NMR spectra were acquired with a Varian Inova 500 MHz instrument operating at 500 MHz and 125 MHz for ^{1}H and ^{13}C spectra, respectively, using $CDCl_3$ (Aldrich, 99.8 atom % D). NMR spectra were recorded at 20 °C, and the chemical shifts were assigned in ppm using TMS δ(0.00) and TMS δ(0.0) as a reference, for ^{1}H and ^{13}C NMR experiments, respectively. Absorption spectra were collected with a Jasco V-670 UV/Vis spectrometer with HPLC grade chloroform (Baker, ≥99.9%), or toluene (Aldrich, 99.8%), used without further purification. Emission data were acquired on a PTI Fluorometer with slit widths of .5 mm using

HPLC grade chloroform (Baker, ≥99.9%) used without further purification. POM was performed on an Olympus BX51 microscope. Centrifugation was performed with a Sorvall MX 150 micro-ultracentrifuge. Bis-C_8 (**1**) and Bis-4hexyl (**2**), and PMADE (**11)** were prepared according to literature procedures.[1,2]

Experimental Procedures

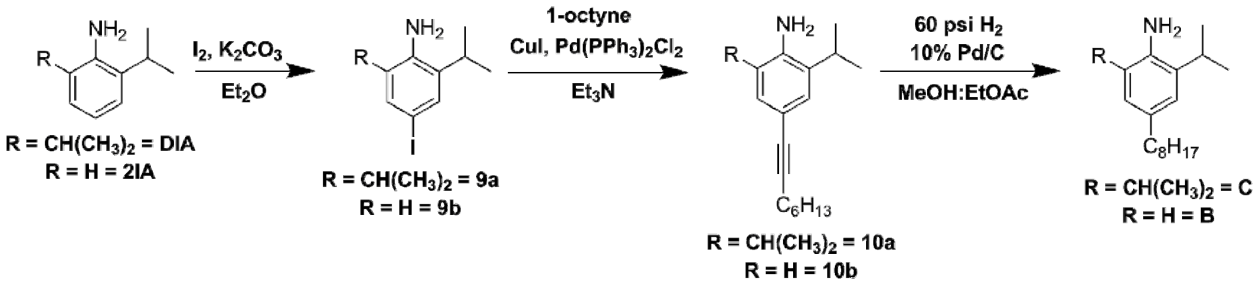

2,6-diisopropyl-4-iodoaniline (9a). In a 250 mL single-necked flask, potassium carbonate (16.5 g, 119 mmol), iodine (13.2 g, 52 mmol), and 2,6-diisopropylaniline (10.1 g, 57 mmol) were added to 100 mL of diethyl ether. The reaction mixture was flushed with N_2 and stirred at room temperature for 16 h with the exclusion of light. After 16 h under N_2, the reaction mixture containing a dark liquid and white solid were rinsed into a separatory funnel with diethyl ether and washed with water, 5% sodium bisulfite, and water. The organic fraction was retained and then dried over magnesium sulfate before the solvent was removed via rotary evaporation. The crude product was purified by column chromatography on silica with CH_2Cl_2:hexanes (70:30) to give **9a** (12.96 g, 85.8%): ^{1}H NMR (500 MHz, $CDCl_3$) δ = 7.20 (s, 2H), 2.76 (septet, J = 6.5 Hz, 2H), 1.15 (d, J = 7 Hz, 12H).

4-iodo-2-isopropylaniline (9b). **9b** was synthesized according to the methods described for **1a** with 2-isopropylaniline (7.70 g, 57 mmol) to give **9b** (10.32 g, 72.43%): ^{1}H NMR (500 MHz, $CDCl_3$) δ = 7.27 (d, *J* = 2 Hz, 1H), 7.17 (dd, *J* = 6, 2 Hz, 1H), 6.32 (d, *J* = 8 Hz, 1H), 3.55 (br s, 2H), 2.69 (septet, *J* = 7 Hz, 1H), 1.12 (d, *J* = 7 Hz, 6H).

2,6-diisopropyl-4-octynylaniline (10a). In a 250 mL round-bottom flask, **9a** (12.05 g, 40 mmol), bis(triphenylphosphine) palladium (II) dichloride (292 mg, 416 μmol) and copper (I) iodide (80 mg, 420 μmol) were added to 150 mL of triethylamine under N_2. Then with the exclusion of light, 1-octyne (9.42 g, 85 mmol) was added drop-wise to the reaction mixture over a 2 h period. Following a 20 h reaction period under N_2, the copper chloride salt was separated from the reaction mixture via vacuum filtration. Next, the dark brown filtrate was reduced to a brown oil via rotatory evaporation. The crude product was purified by column chromatography on silica with CH_2Cl_2:hexanes (70:30) to give **10a** (7.35 g, 61.9%): ^{1}H NMR (500 MHz, $CDCl_3$) δ = 7.01 (s, 2H), 3.72 (br s, 2H), 2.69 (septet, *J* = 7 Hz, 2H), 2.31 (t, *J* = 7.5 Hz, 2H), 1.52 (quintet, *J* = 7.5 Hz, 2H), 1.37 (m, 2H), 1.24 (m, 4H), 1.16 (d, *J* = 7 Hz, 12H), 0.82 (t, *J* = 7 Hz, 3H).

4-octynyl-2-isopropylaniline (10b). **10b** was synthesized according to the methods described for **10a** with **9b** (10.32 g, 40 mmol) to give **10b** (8.49 g, 86.9%): ^{1}H NMR (500 MHz, $CDCl_3$) δ = 7.10 (d, *J* = 2 Hz, 1H), 6.98 (dd, *J* = 8.5, 2 Hz, 1H), 6.46 (d, *J* = 8 Hz, 1H), 3.62 (s, 2H), 2.73 (septet, *J* = 7 Hz, 1H), 2.30 (t, *J* = 7.5 Hz, 2H), 1.50 (quintet, *J* = 7.5 Hz, 2H), 1.36 (quintet, *J* = 5 Hz, 2H), 1.24 (m, 4H), 1.14 (d, *J* = 7 Hz, 6H) 0.82 (t, *J* = 7 Hz, 3H).

2,6-diisopropyl-4-octylaniline (C). In a 250 mL Fisher-Porter tube, **10a** (10.13 g, 36 mmol) and 500 mg of the heterogeneous catalyst 10% Pd on carbon was added to 10 mL of MeOH in a nitrogen atmosphere glovebox. The reaction vessel was then pressurized to 60 psi with UHP H_2 and stirred vigorously. The reaction vessel was pressurized to 60 psi repeatedly over a 4 h period until the consumption of H_2 had ceased. Once H_2 consumption had stopped, the catalyst was removed from the reaction mixture by filtration through a bed of silica with methanol as the eluent. The eluent was collected and the solvent was removed under reduced pressure to give **C** as a light brown oil (9.30 g, 91.3%). ^{1}H NMR (500 MHz, $CDCl_3$) δ = 6.78 (s, 2H), 3.54 (br s, 2H), 2.86 (septet, J = 7 Hz, 2H), 2.44 (t, J = 8 Hz, 2H), 1.50 (m, 4H), 1.24 (m, 8H), 1.14 (d, J = 7 Hz, 12H), 0.81 (t, J = 7 Hz, 3H).

4-octyl-2-isopropylaniline (B). **B** was synthesized according to the methods described for **C** with **10b** (10.40 g, 43 mmol) to give **B** (9.37 g, 89.4%): ^{1}H NMR (500 MHz, $CDCl_3$) δ = 6.87 (d, J = 2 Hz, 1H), 6.76 (dd, J = 8, 2 Hz, 1H), 6.54 (d, J = 7.5 Hz, 1H), 3.46 (br s, 2H), 2.83 (septet, J = 7 Hz, 1H), 2.42 (t, J = 8 Hz, 2H), 1.48 (quintet, J = 8 Hz, 4H), 1.23 (m, 8H), 1.18 (d, J = 7 Hz, 6H), 0.81 (t, J = 7.5 Hz, 3H).

Bis-G_8 (7).

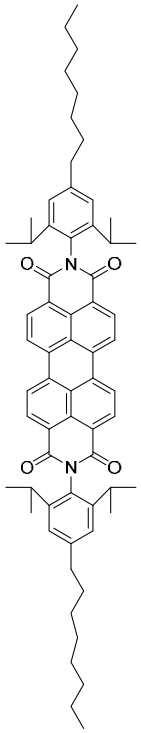

In a 50 mL round-bottom flask equipped with a stir bar, zinc acetate (477 mg, 2.6 mmol) and perylene-3,4:9,10-tetracarboxylicanhydride (PBA) (1.0 g, 2.5 mmol) was added to 20 g of molten imidazole at 110 °C. After a homogeneous solution was achieved, **C** (7.37 g, 25 mmol) was added drop-wise to the reaction mixture. The reaction mixture was then put under a N_2 atmosphere before being slowly ramped to 180 °C and left to stir for 16 h. After being cooled to 110 °C, the reaction was quenched with 30 mL of 2M HCl before being poured into 300 mL of MeOH:HCl (2:1) and left to stir overnight. After vacuum filtration, the dark purple solid was purified by column chromatography on silica with CH_2Cl_2:EtOAc (20:1) to give **7** as a red solid (314 mg, 31.4%): ^{1}H NMR (500 MHz, $CDCl_3$) δ = 8.72 (d, *J* = 8 Hz, 4H), 8.67 (d, *J* = 7.5 Hz, 4H), 7.08 (s, 4H), 2.63 (m, 4H), 1.64 (m, 4H), 1.36-1.24 (m, 10H), 1.11 (d, *J* = 7 Hz, 20H), 0.84

(t, J = 6.5 Hz, 6H) ^{13}C NMR (125 MHz, $CDCl_3$) δ = 164, 145, 144, 135, 132, 130, 128, 127, 124, 123, 123, 36, 32, 31, 30, 30, 29, 29, 24, 23, 14 ppm. λ_{abs}=527 nm, λ_{em}=533 nm.

Bis-D_8 (4).

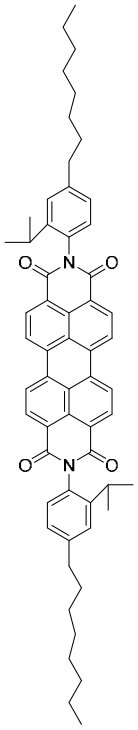

4 was synthesized according to the methods described for **7** with zinc acetate (477 mg, 2.6 mmol), PBA (1.0 g, 2.5 mmol), and **B** (6.30 g, 25 mmol) to give **4** (353 mg, 35.3%): ^{1}H NMR (500 MHz, $CDCl_3$) δ = 8.70 (d, J = 8.5 Hz, 4H), 8.64 (d, J = 8 Hz, 4H), 7.19 (s, 2H), 7.12 (d, J = 8 Hz, 2H), 7.02 (d, J = 8 Hz, 2H), 2.72 (septet, J = 6.5 Hz, 2H), 2.63 (t, J = 8 Hz, 4H), 1.63 (quintet, J = 7.5 Hz, 4H), 1.35-1.23 (m, 20H), 1.13 (d, J = 7 Hz, 12H), 0.83 (t, J = 5 Hz, 6H) ^{13}C NMR (125 MHz, $CDCl_3$) δ: 163.7, 145.7, 144.3, 135.0, 132.0, 130.3, 130.0, 128.1, 127.1, 126.8, 126.7, 123.6, 123.3, 36.1, 32.0, 31.3, 29.6, 29.3, 28.7, 23.8, 22.7, 14.2 ppm. λ_{abs} = 527 nm, λ_{em} = 532 nm.

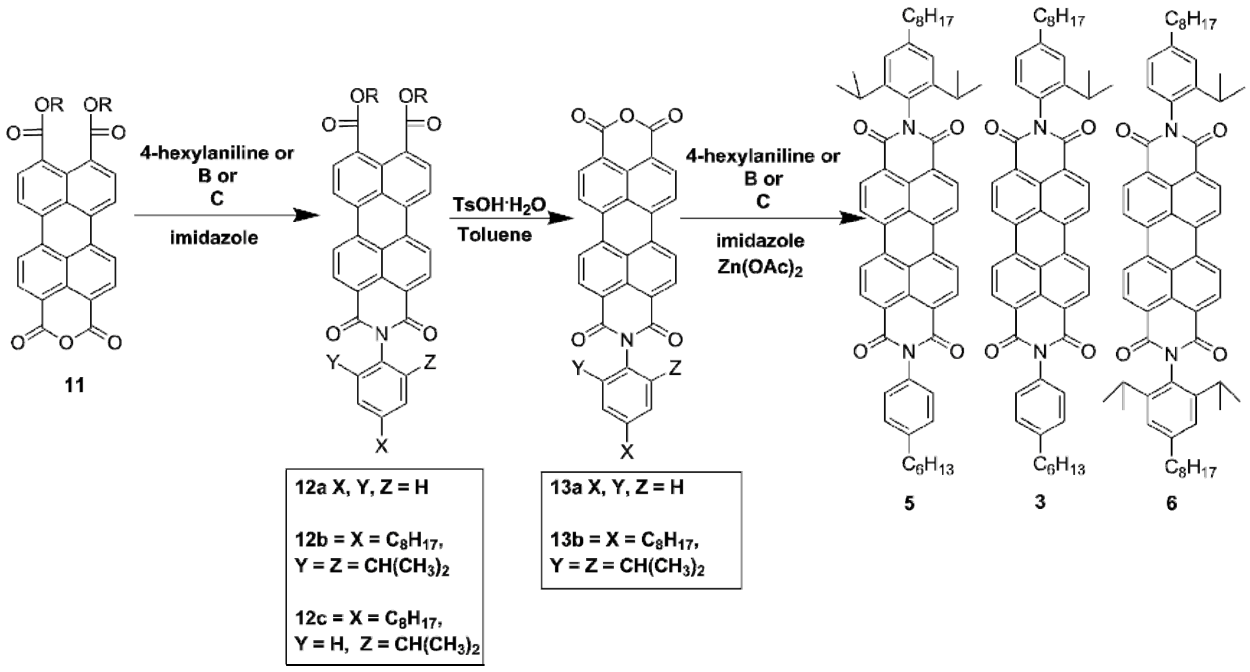

4-hexyl-DE (12a). In a 50 mL round-bottom flask equipped with a stir bar, **11** (4.9 g, 7 mmol) was added to 22.5 g of molten imidazole at 110 °C. 4-hexylaniline (2.2 g, 12 mmol) was then added drop-wise to the reaction mixture before being slowly heated to 130 °C and stirred under N_2 for 3 h. After cooling to 110 °C, the dark red solution was quenched with 30 mL of deionized H_2O and stirred vigorously for 10 m. Next, the reaction mixture was poured into 100 mL of deionized water and stirred for an additional 2 h before recovering a brick red solid via vacuum filtration. Following a light rinse with hexanes, the crude product was purified by column chromatography on silica with CH_2Cl_2: EtOAc (20:1) to give **12a** (3.90 mg, 67.1%): ^{1}H NMR (500 MHz, $CDCl_3$) δ = 8.79 (d, *J* = 7.5 Hz, 4H), 8.74 (d, *J* = 8.5 Hz, 4H), 7.15 (s, 2H), 2.74-2.67 (m, 4H), 1.71 (quintet, *J* = 8 Hz, 2H), 1.44-1.31 (m, 10H), 1.18 (d, *J* = 6.5 Hz, 12H), 0.91 (t, *J* = 7 Hz, 3H).

G_8-DE (12b). **12b** was synthesized according to the methods described for **12a** with **C** (2.2 g, 12 mmol) to give **12b**: ^{1}H NMR (500 MHz, $CDCl_3$) δ = 8.79 (d, *J* = 7.5 Hz, 4H), 8.74 (d, *J* = 8.5 Hz, 4H), 7.15 (s, 2H), 2.74-2.67 (m, 4H), 1.71 (quintet, *J* = 8 Hz, 2H), 1.44-1.31 (m, 10H), 1.18 (d, *J* = 6.5 Hz, 12H), 0.91 (t, *J* = 7 Hz, 3H).

4-hexyl-MA (13a). To a 250 mL round-bottom flask equipped with a stir bar, 100 mL of toluene was added and brought to 80 °C. Next, **12a** (890 mg, 1 mmol) was added along with p-toluenesulfonic acid monohydrate (1.19 g, 6 mmol) and the reaction mixture was slowly heated to 100 °C, capped with a rubber septa and stirred under N_2 for 2 h. After cooling to room temperature, an insoluble bright red solid was acquired via vacuum filtration. Following a trituration in hexanes the crude product was used without characterization.

G_8-MA (13b). **13b** was synthesized according to the methods described for **13a** with **12b** (850 mg, 1 mmol) to give **13b** as a dull red solid. Following a trituration in hexanes, the crude product was used without further purification.

G_8-4hexyl (5).

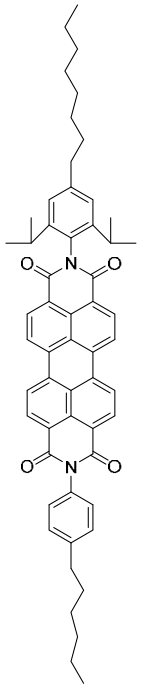

5 was synthesized according to the methods described for **7** with **13a** (1.1 g, 2 mmol), zinc acetate (385 mg, 2.1 mmol), and **C** (1.73 g, 6 mmol) to give **5** as a dull red solid. The crude product was purified using column chromatography over silica gel with DCM to give **5** as a purple solid. ^{1}H NMR (500 MHz, $CDCl_3$) δ: 8.79 (d, J = 8 Hz, 2 H), 8.76 (d, J = 7.5 Hz, 2 H), 8.72 (dd, J = 8 Hz), (d, J = , 2 H), (d, J = , 2 H), 7.15 (s,2 H), 2.76-2.67 (m, 6 H), 1.74-1.66 (m, 4 H), 1.45-1.26 (m, 16 H), 1.18 (d, J = 6.5 Hz, 12 H), .94-.89 (m, 6 H). ^{13}C NMR Data (125 MHz, $CDCl_3$) δ: 163.7, 163.6, 145.1, 144.1, 143.8, 135.0, 132.4, 132.0, 131.9, 130.1, 129.9, 129.5, 128.2, 128., 126.8, 126.7, 124.2, 123.6, 123.3, 36.3, 35.8, 31.9, 31.8, 31.3, 31.2, 29.7, 29.5, 29.3, 29.2, 24.0, 22.7, 14.2 ppm. λ_{abs} = 527 nm, λ_{em} = 533.

D_8-4hexyl (3).

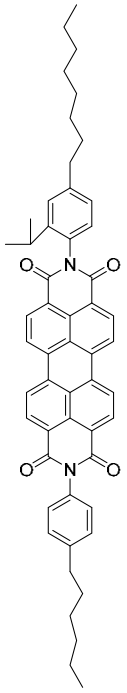

3 was synthesized according to the methods described for **7** with **13a** (1.1 g, 2 mmol), zinc acetate (385 mg, 2.1 mmol), and **B (**1.49 g, 6 mmol) to give **3** as a dull red solid. The crude product was purified using column chromatography over silica gel with dichloromethane. ^{1}H NMR (500 MHz, $CDCl_3$) δ = 8.70 (dd, J = 7.5, 1.6 Hz, 4H), 8.64 (d, J = 8.5 Hz, 4H), 7.32 (d, J = 8.5 Hz, 2H), 7.25 (d, J = 2 Hz, 1H), 7.18 (d, J = 6.5 Hz, 2H), 7.12 (dd, J = 5, 2 Hz, 1H), 7.03 (d, J = 8.5 Hz, 1H), 2.71 (septet, J = 6.5 Hz, 1H), 2.64 (q, J = 8 Hz, 2H), 1.63 (quintet, J = 8 Hz, 2H), 1.35-1.18 (m, 20H), 1.13 (d, J = 6.5 Hz, 6H), 0.84 (m, 6H) ^{13}C NMR (125 MHz, $CDCl_3$) δ: 163.7, 145.7, 144.3, 143.8, 135.0, 134.9, 132.4, 131.9, 130.3, 130.0, 129.8, 129.5, 128.2, 127.1, 126.8, 123.6, 123.3, 36.1, 35.8, 31.9, 31.8, 31.2, 29.5, 29.3, 29.1, 28.7, 23.7, 22.7, 14.1 ppm. λ_{abs} = 528 nm, λ_{em} = 534 nm.

D_8-G_8 (6).

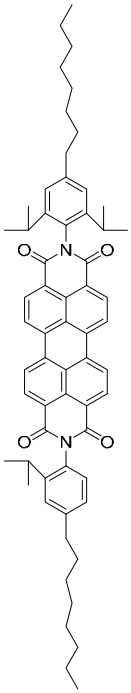

6 was synthesized according to the methods described for **7** with **13b** (1.25 g, 2 mmol), zinc acetate (385 mg, 2.1 mmol) and **B** (1.73 g, 6 mmol) to give **6** as a dull red solid. The crude product was purified using column chromatography over silica gel using dichloromethane. ^{1}H NMR (500 MHz, $CDCl_3$) δ = 8.78 (dd, J = 7.7, 3.5 Hz, 4H), 8.74 (d, J = 8 Hz, 4H), 7.32 (s, 1H), 7.19 (d, J = 6.5 Hz, 1H), 7.15 (s, 2H), 7.09 (d, J = 7.5 Hz, 1H), 2.79 (septet, J = 7 Hz, 1H), 2.70 (septet, J = 8 Hz, 2H), 1.71 (quintet, J = 8 Hz, 2H), 1.42-1.25 (m, 24H), 1.21 (d, J = 6.5 Hz, 6H), 1.17 (d, J = 6.5 Hz, 12H), 0.91 (m, 6H) ^{13}C NMR (125 MHz, $CDCl_3$) δ: 163.7, 163.6, 145.7, 145.1, 144.3, 144.1, 135.0, 132.1, 132.0, 130.3, 130.1, 130.0, 128.0, 127.1, 126.8, 126.7, 124.2, 123.6, 123.5, 123.3, 36.3, 36.1, 32.0, 31.3, 29.7, 29.6, 29.5, 29.4, 29.3, 29.2, 28.7, 24.0, 23.7, 22.7, 14.2 ppm. λ_{abs} = 528 nm, λ_{em} = 532 nm.

Quantum Yield Calculations. The quantum yields of the dyes synthesized in this study were calculated using the single point method. This method uses a compound of known FQY as a reference compound to calculate the FQY of the unknown (Eq. 1).

$$Q = Q_R \frac{I}{I_R} \frac{OD_R}{OD} \frac{n^2}{n_R^2} \quad (1)$$

In equation 1: Q_R represents the FQY of the reference compound, I is the integrated fluorescence intensity, OD is the optical density (absorbance) at the excitation wavelength and n is the refractive index of the solvent. For the classes of compounds studied, LumO derivatives, the parent compound from BASF was used as the reference. Each measurement was taken in chloroform with optical densities less than 0.2 to ensure that there was no fluorescence quenching due to aggregation.

Solubility Calculations. The solubility of the dyes in the LC matrix 5CB was determined by using Beer's Law and the extinction coefficient determined through quantum yield measurements in chloroform. This calculation assumes no contribution from the small amount of LC present. Because PBIs are known for their low solvatochromism it is assumed that there is no change in the molar absorptivity from chloroform to toluene. Determination of the dye's solubility begins with the addition of ~25 mg of dye to .5 g of LC solution (density = 1.008 g/mL).

After a sonication, ultracentrifugation, and filtration to obtain a saturated solution, 50 μL were removed and added to 100 mL volumetric flask that is then brought to mark with toluene. An absorption spectrum was acquired, and the concentration was calculated by a rearrangement

of Beer's law with the extinction coefficients calculated in chloroform with ε equal to 75,000 for the LumO (Eq. 2 and Eq. 3).

$$A = \varepsilon bc \tag{2}$$

$$\frac{A}{\frac{L}{mol \cdot cm} \cdot cm} = c \tag{3}$$

The concentration of dye in the original saturated LC solution was then determined by taking the product of the Beer's law concentration (C), the dilution factor (DF), the volume of toluene (L), and converting it into grams using the specific dyes molecular weight (MW) (eq. 4).

$$(C \cdot DF \cdot 0.010\ L) \cdot MW = g\ of\ dye\ in\ saturated\ LC\ solution \tag{4}$$

Orientational Order Parameter Measurements in 5CB.

Planar LC cells formed from two glass coverslips coated on their inner surfaces with mechanically rubbed poly(vinylalcohol) were filled with a solution of dye and the nematic liquid crystal 4'-pentyl-4-cyanobiphenyl. The scalar order parameter was computed from measurements of the peak absorbance using plane polarized light parallel $A_{\parallel}$ and perpendicular $A_{\perp}$ to the rubbing direction:

$$S = \frac{A_{\parallel} - A_{\perp}}{A_{\parallel} + 2A_{\perp}}, \tag{5}$$

Luminescent Solar Concentrator Fabrication and Characterization

A 1:2 mass:mass mixture was prepared of the polymerizable liquid crystal RMM28A (Merck) and a toluene solution containing 3217 ppm Irgacure 651 (Ciba AG), a photoinitiator. To this solution enough D8 was added to give a dye concentration of 333 ppm. After thorough mixing the solution was spin cast onto borosilicate glass coverslips and the toluene evaporated under a stream of nitrogen, giving a final dye concentration in the polymer film of 1000 ppm. Upon evaporation of toluene RMM28A enters a liquid crystalline phase at room temperature; this phase is metastable toward crystallization, so must be promptly polymerized. Polymerization was performed with illumination from a mercury arc lamp under a stream of nitrogen, producing a solid film. RMM28A contains an aliphatic alcohol surfactant causing films prepared in this way to possess homeotropic orientation. RMM28A is birefringent, with refractive indices reported by the manufacture $n_o = 1.525$ and $n_e = 1.667$. The polymer layer was 1 – 5 μm thick, resulting in a peak absorbance of 0.0039 at 534 nm for the sample reported here. All device edges except for a small aperture through which light was collected were then blackened with paint. Samples measured 2.5 x 2.5 x 0.16 cm in size, resulting in a geometric gain, defined as the facial-to-edge area ratio, $G = 10$.

To determine OQE two corrections to the measured edge emission intensity are required accounting for the fact that: (1) light from only a portion of the whole perimeter was collected, and (2) only a certain fraction of photons reaching the device edge could be detected with our experimental arrangement because some photons travel in directions lying outside the edge escape cone. Such photons are reflected back into the device, rather than being detected. Note that in actual application the LSC would have perimeter-attached

photovoltaic cells whose refractive index exceeded that of the glass substrate and the polymer layers (e.g. Si); under such conditions all photons reaching the edge could in principle be captured. Efficiency is computed as:

$$\mathrm{OQE} = fN_{em}/N_{abs}, \quad (6)$$

where N_{em} is the number of photons collected from the edge aperture, $N_{abs} = P_{ex}\lambda/hc(1 - 10^{-A})$ is the number of photons absorbed by the sample (P_{ex} and λ are the power and wavelength of the excitation source, A is the LSC absorbance at the excitation wavelength, h is Planck's constant and c is the speed of light), and $1/f$ is the fraction of photons reaching the perimeter that arrive within the collection aperture traveling within the edge escape cone. It represents the ratio of the number of photons that are detected using our experimental arrangement to the number that would have been detected if photovoltaic cells had been attached around the full perimeter. Its value is computed via ballistic Monte Carlo simulations employing the model of Ref. 3. This model accounts for the specific absorption and emission profiles of the dyes used, for the stochastic alignment of the absorption dipoles, for the non-zero angle between the absorption and emission dipoles and correctly models dependence of propagation on polarization of photons. The angle β between absorption and emission dipoles was computed from temperature-dependent measurements of the fundamental anisotropy in poly(propylene glycol) according to the procedure in [J. Lakowicz, "Principles of Fluorescence Spectroscopy" 3rd Ed. Springer, 2006, New York]. For **4** this gave $\beta = 16.6°$. Modifications were made to incorporate Lambertian emission direction (the probability of emission direction being proportional to the square of the sine of the angle with the dipole), the Fresnel relations at media interfaces, and the physics of light propagation within a birefringent medium. Photons, distributed uniformly over the top face of the LSC, were initiated with propagation direction perpendicular to this face, with random

polarization in the plane of the face, and absorption within the dye-layer was forced. From simulating hundreds of thousands of such photons we are able to estimate, of all photons which propagate to an edge, what proportion of them meet the collection aperture, and what proportion are within the side-escape-cone. From this we find $f = 23.74$.

Measuring Dye Orientational Order Parameters in Polymerized RMM28A

The order parameter for the absorption transition moment of dye **4** in photo-polymerized RMM28A was measured by polarized UV-Vis absorbance spectroscopy in thin films having planar orientation. To achieve uniform planar orientation, first two glass coverslips were coated by a thin layer of poly(vinylalcohol), which was then rubbed with a velvet shim. A mixture of RMM28A containing approximately 1000 ppm dye was then prepared heated to a temperature of about 50 °C. At this temperature RMM28A forms a nematic phase, which adopts planar orientation on rubbed PVA. A cell was assembled by adding the second PVA-coated coverslip, and when a uniform planar texture had been achieved (as confirmed by polarizing optical microscopy), the cell was polymerized with a mercury arc lamp under a stream of nitrogen. During this process care must be taken to maintain the LC in its nematic phase, since upon cooling to room temperature a different metastable LC phase is induced (presumed to be smectic-A) and the quality of alignment on rubbed PVA-coated glass is greatly diminished. Order parameter measurements were then performed as described above. Figure S1 shows representative spectra for **4**.

References

[1] J. Lindsey, R. Loewe, P. Thamyongkit and K. Tomizaki, *Tetrahedron* 2003, **59,** 1191-1207.
[2] C. Xue, R. Sun, R. Annab, D. Abadi and S. Jin, *Tetrahedron Lett.* 2009, **50**, 853-856.
[3] S. McDowall, B. L. Johnson and D. L. Patrick, *J. Appl. Phys*., 2010, **108**, 053508.

NMR Spectra

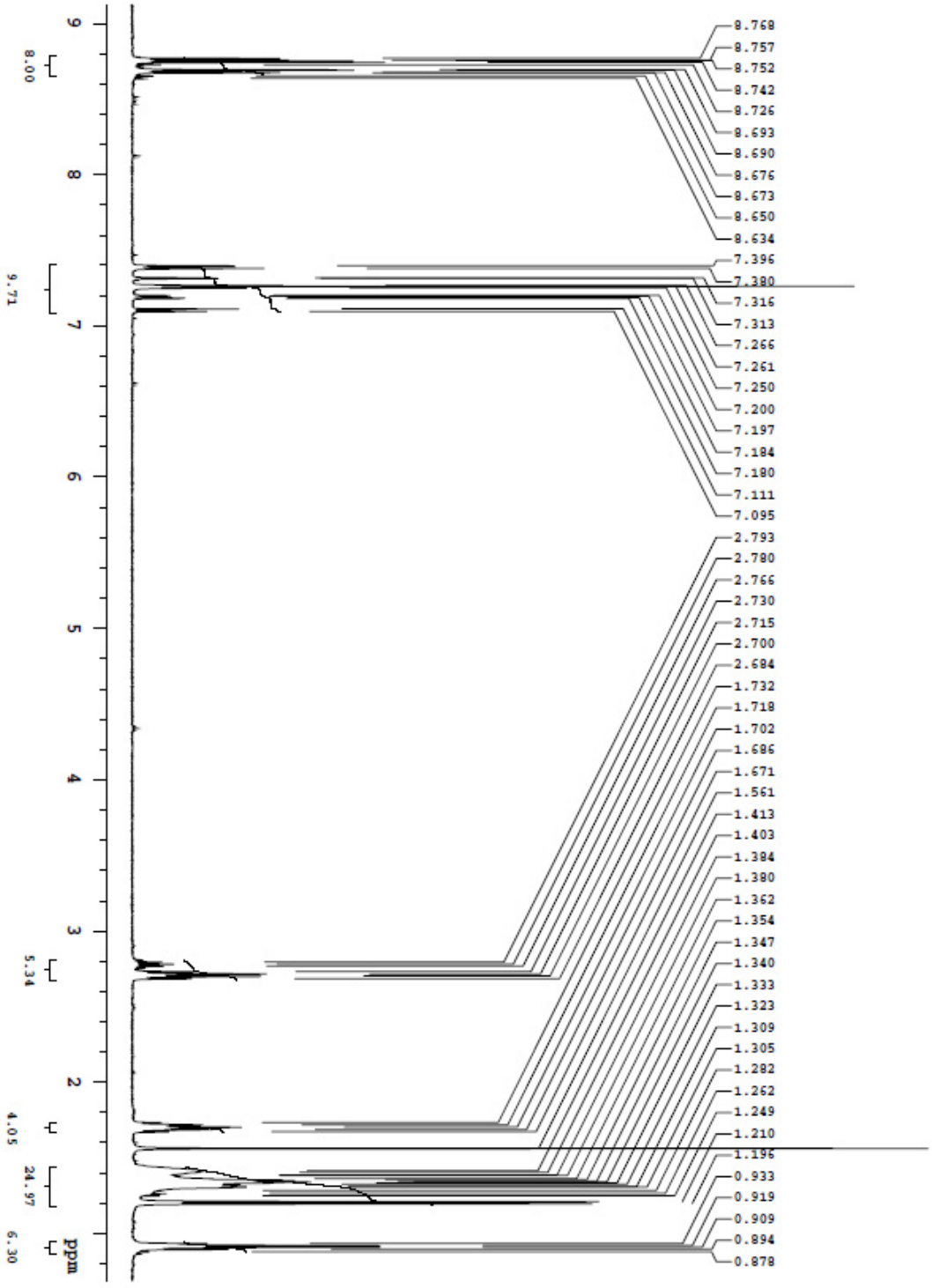

Figure S1. **3** ^{1}H NMR Spectrum in $CDCl_3$.

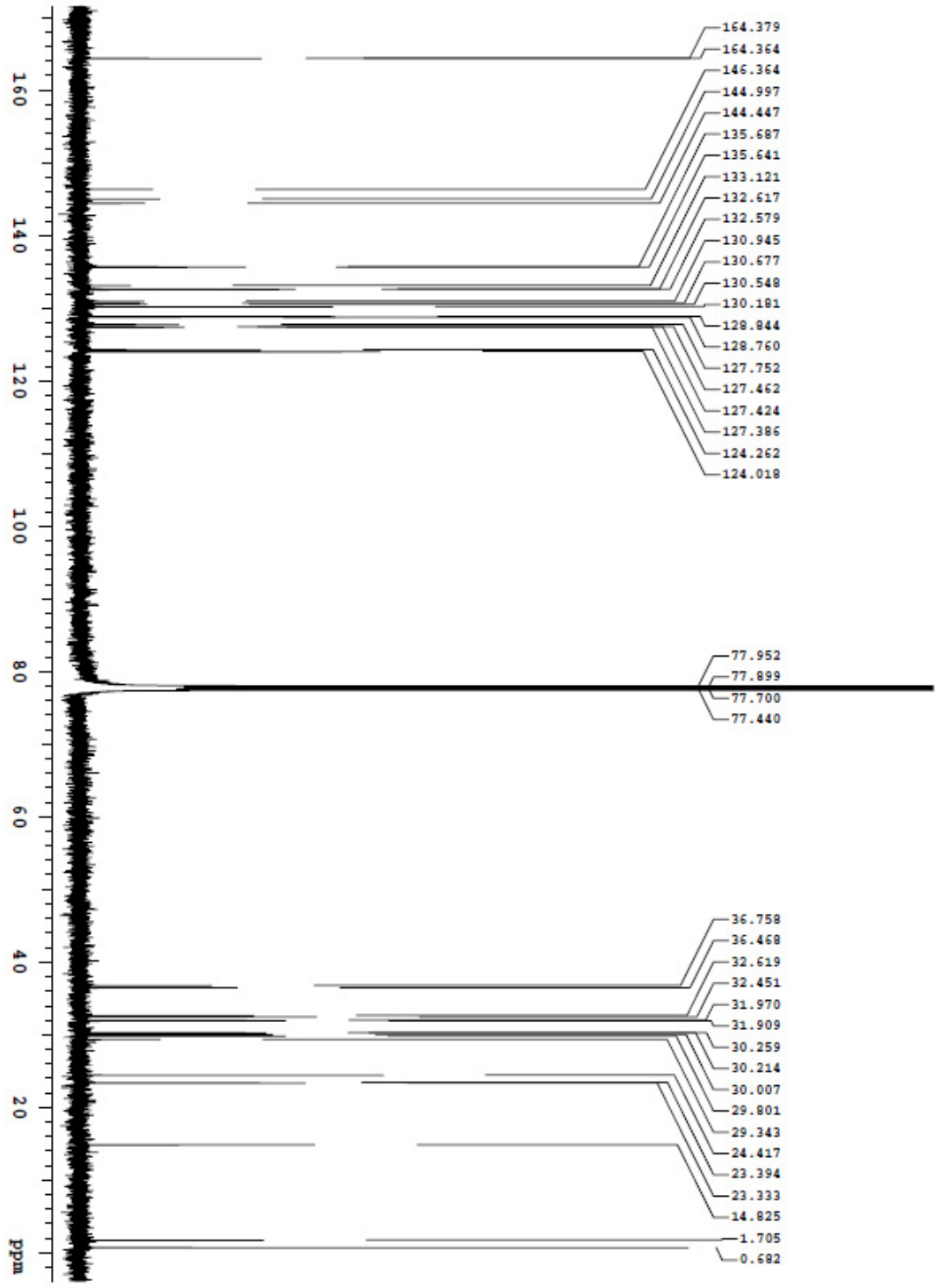

Figure S2. **3** ^{13}C NMR Spectrum in $CDCl_3$.

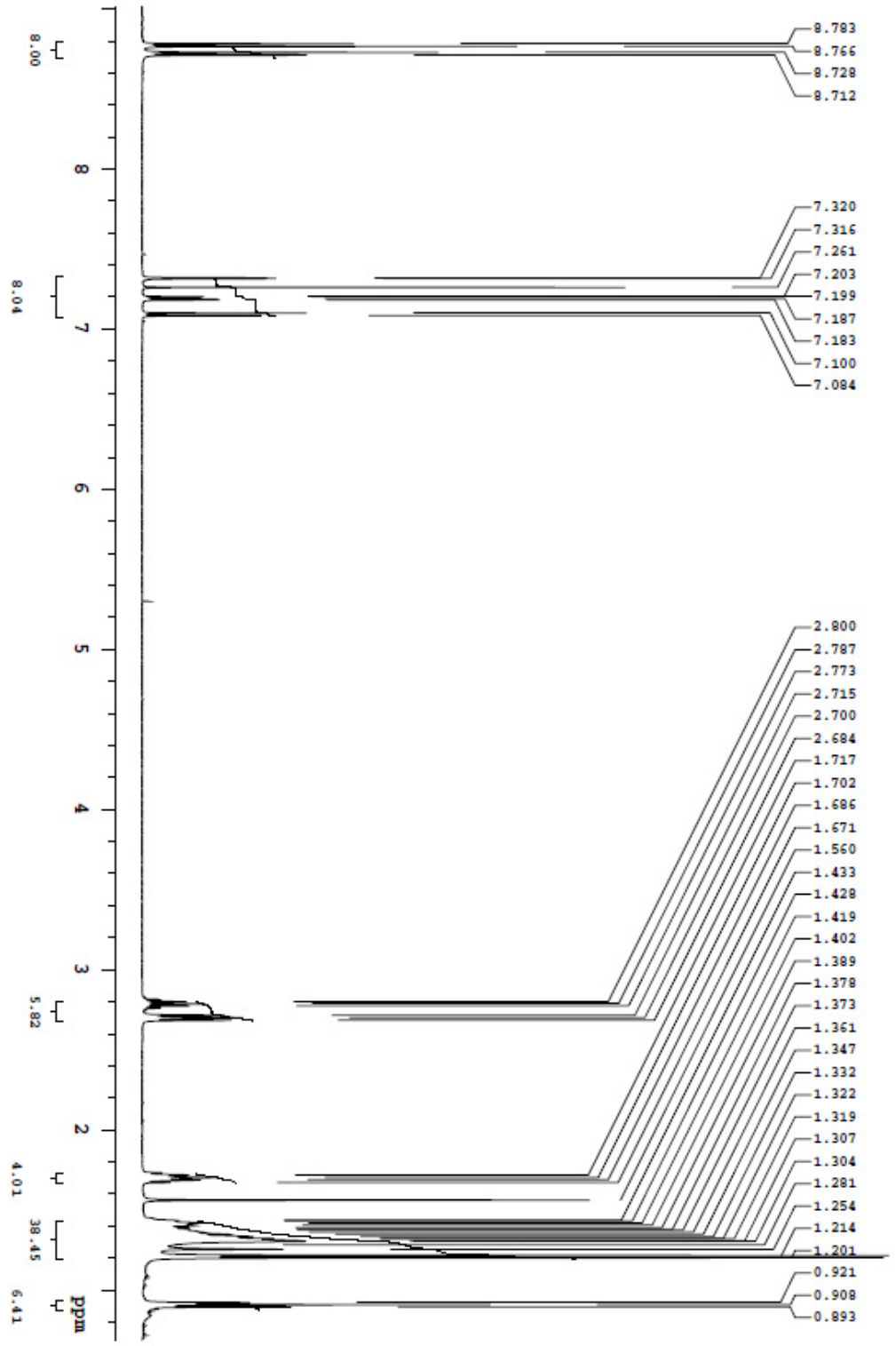

Figure S3. **4** ^{1}H NMR Spectrum in $CDCl_3$.

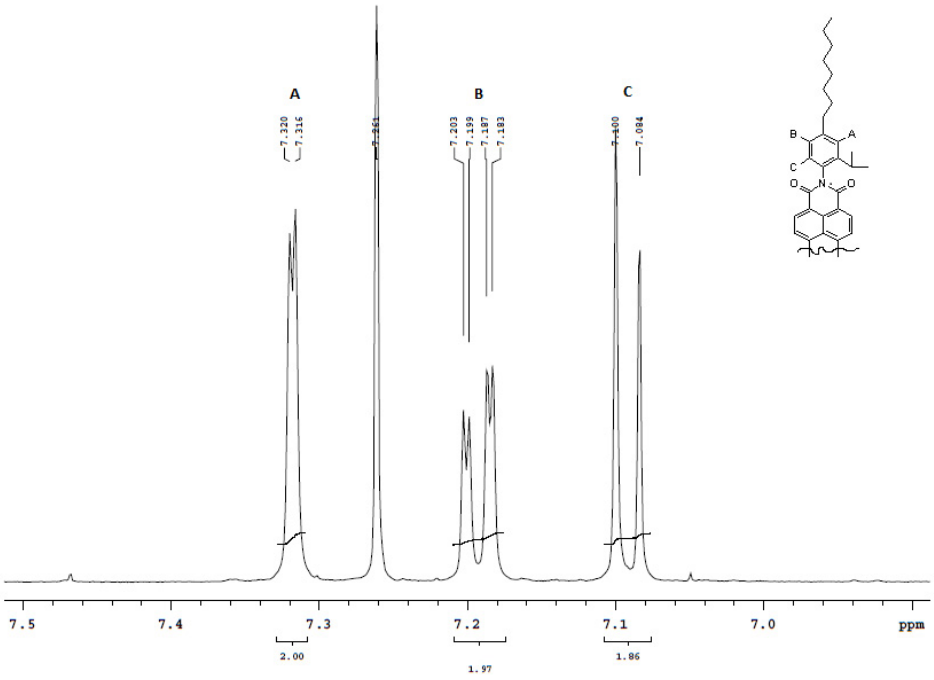

Figure S4. **4** ^{1}H NMR Spectrum 7.4-7.0 ppm in $CDCl_3$.

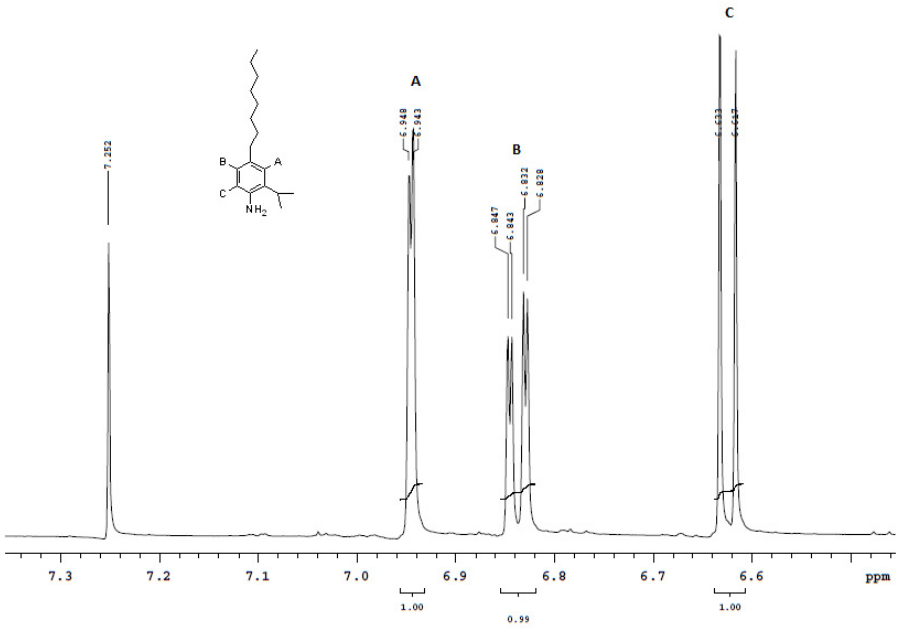

Figure S5. **B** ^{1}H NMR Spectrum in $CDCl_3$.

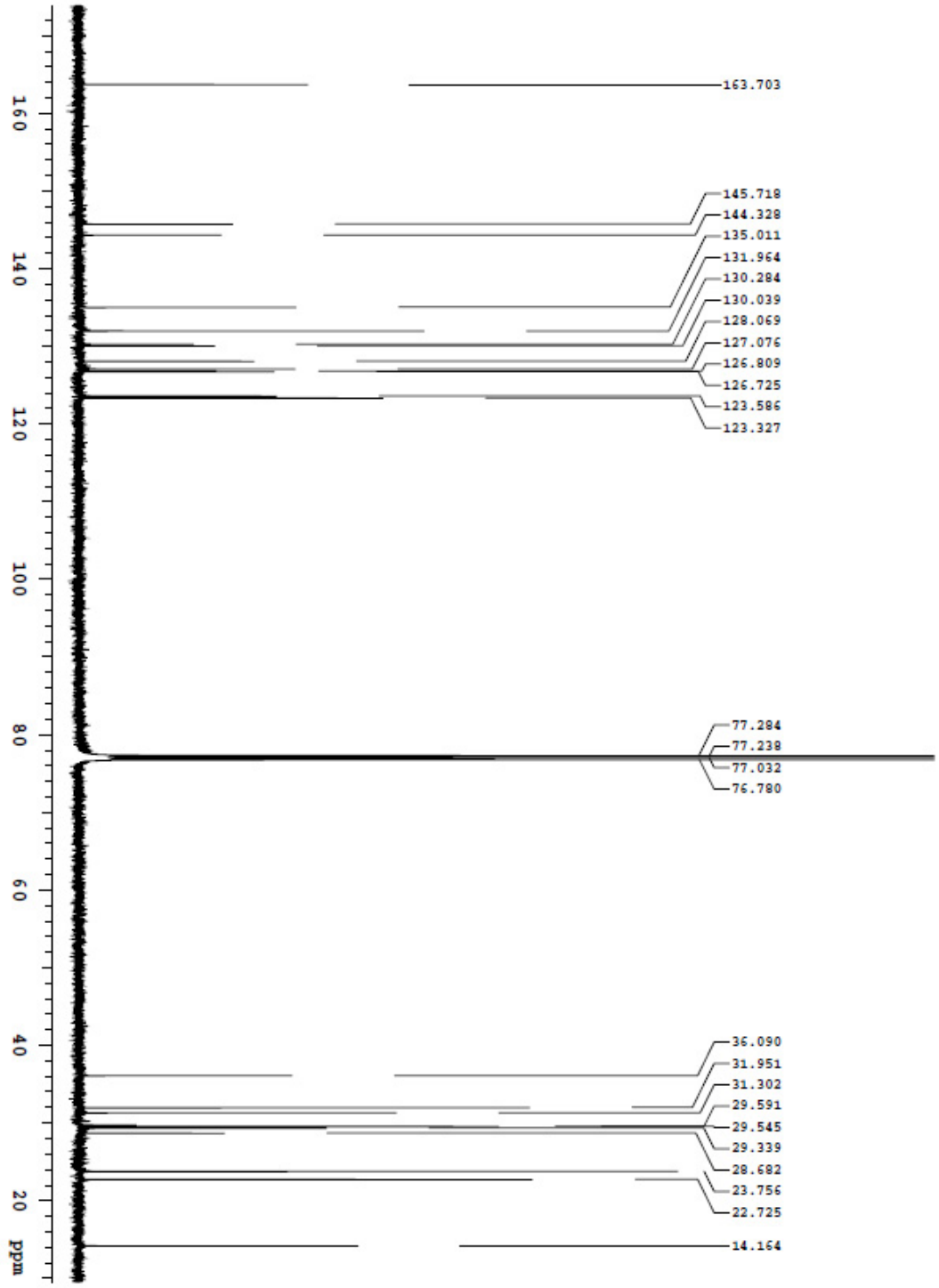

Figure S6. **4** ^{13}C NMR Spectrum in $CDCl_3$.

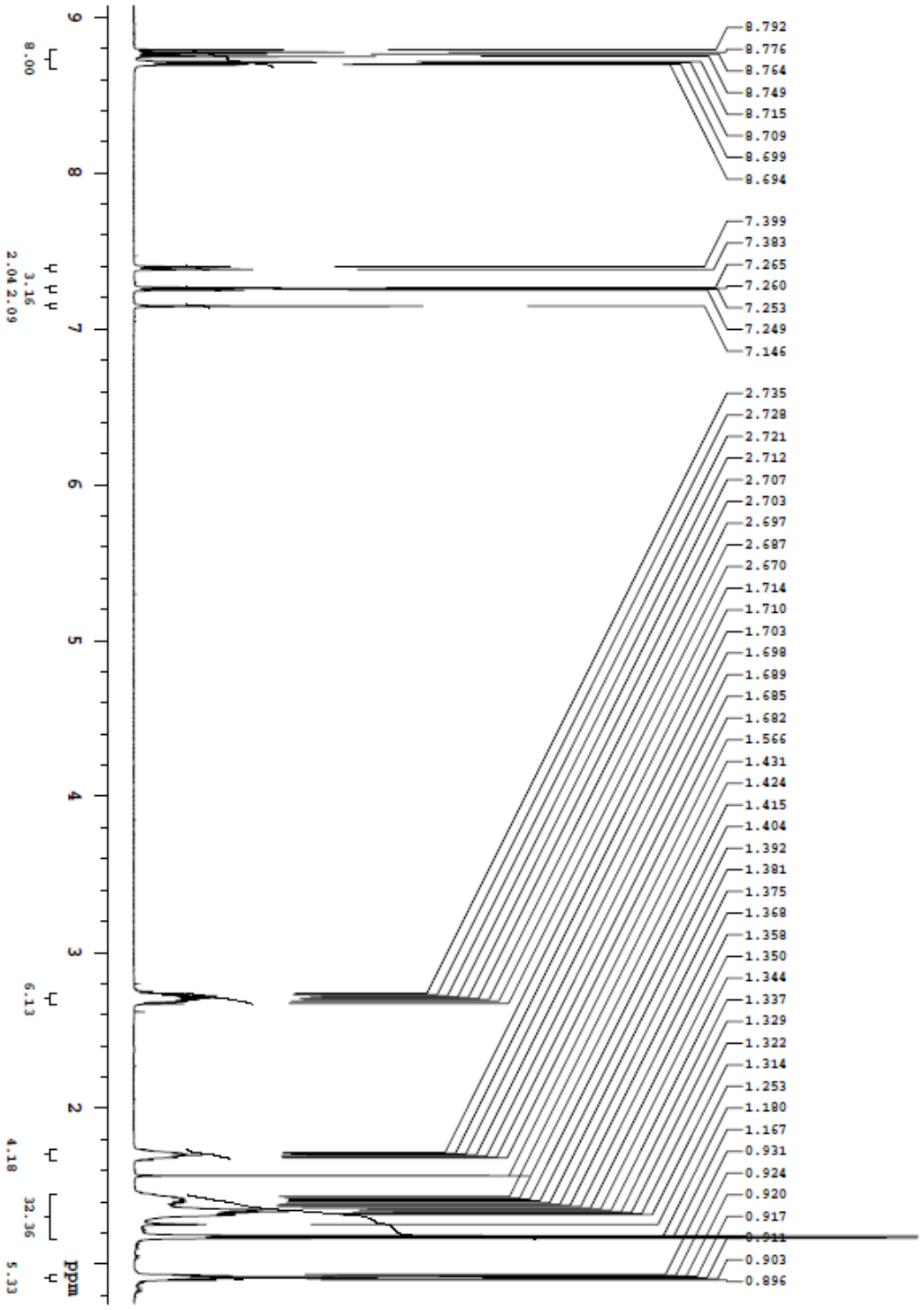

Figure S7. **5** ^{1}H NMR Spectrum in $CDCl_3$.

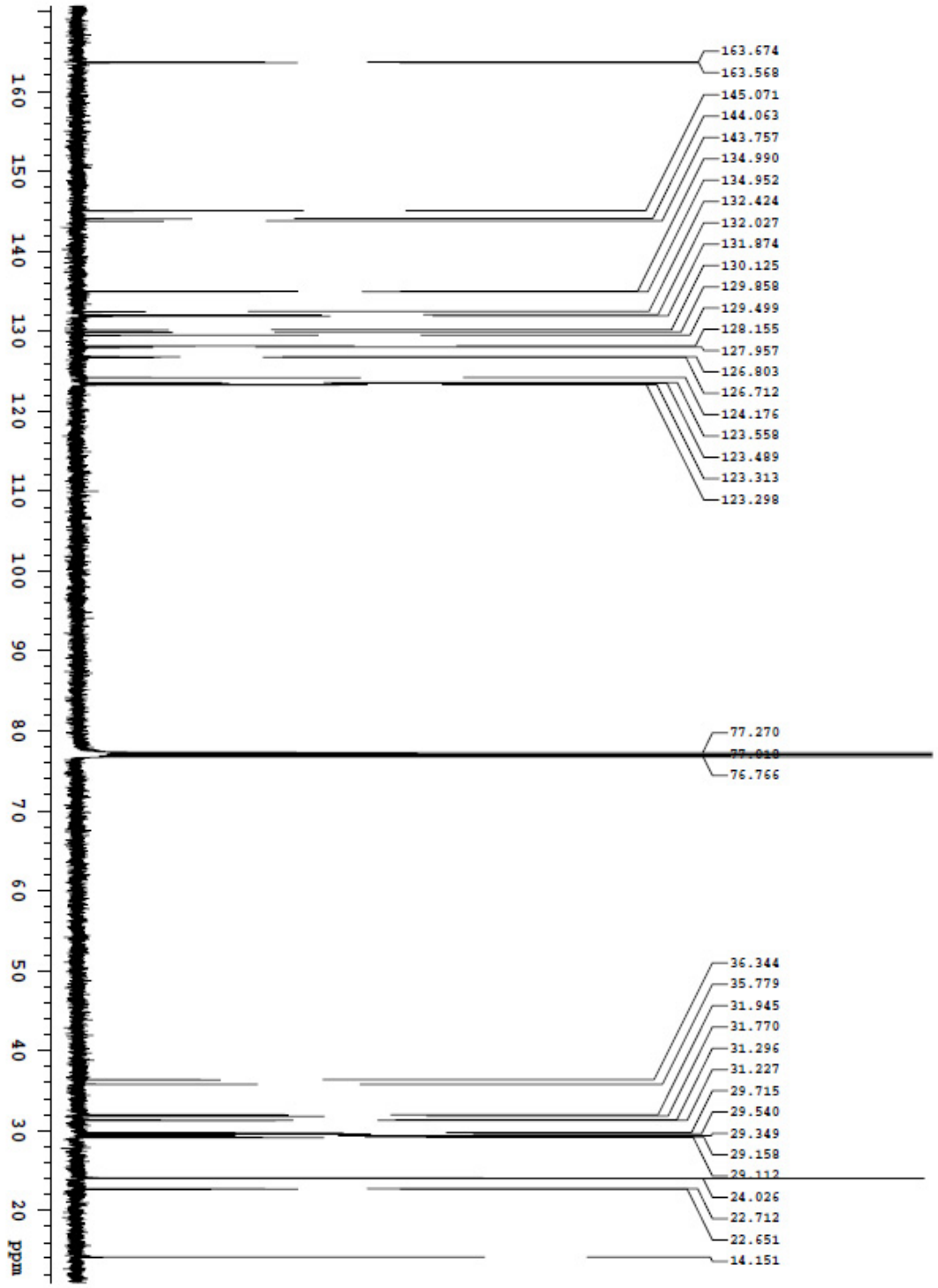

Figure S8. **5** ^{13}C NMR Spectrum in $CDCl_3$.

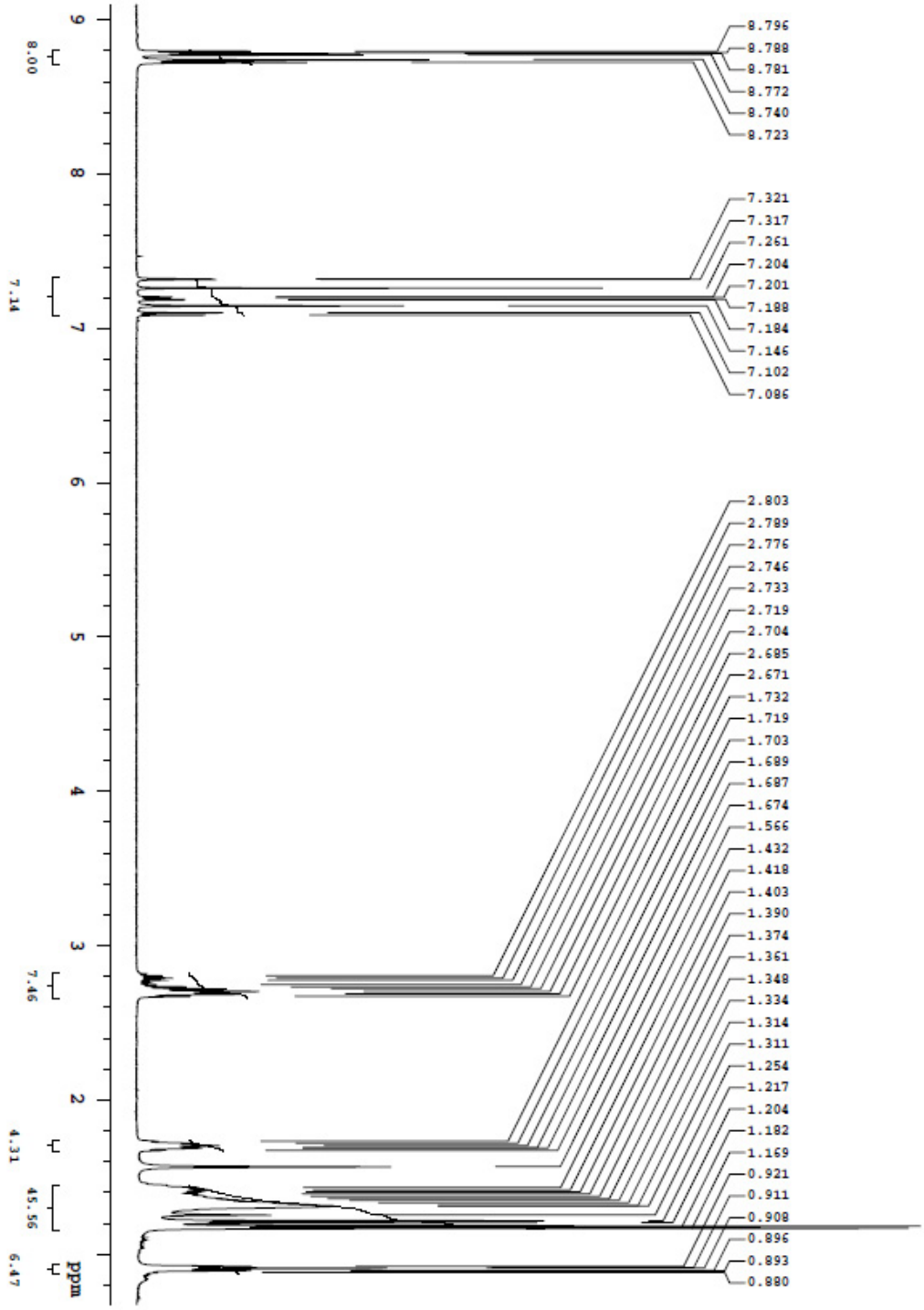

Figure S9. **6** ^{1}H NMR Spectrum in $CDCl_3$.

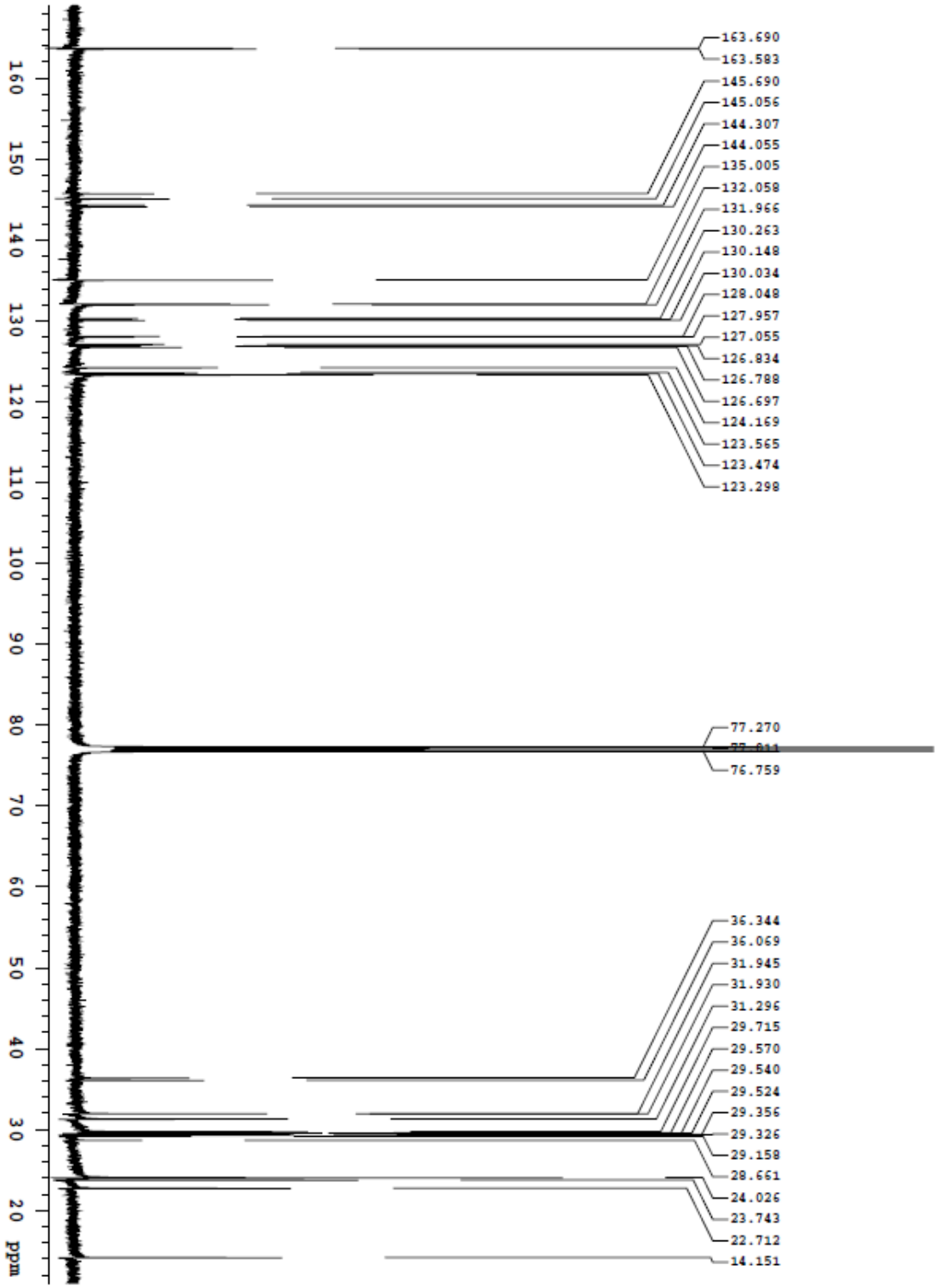

Figure S10. **6** ^{13}C NMR Spectrum in $CDCl_3$.

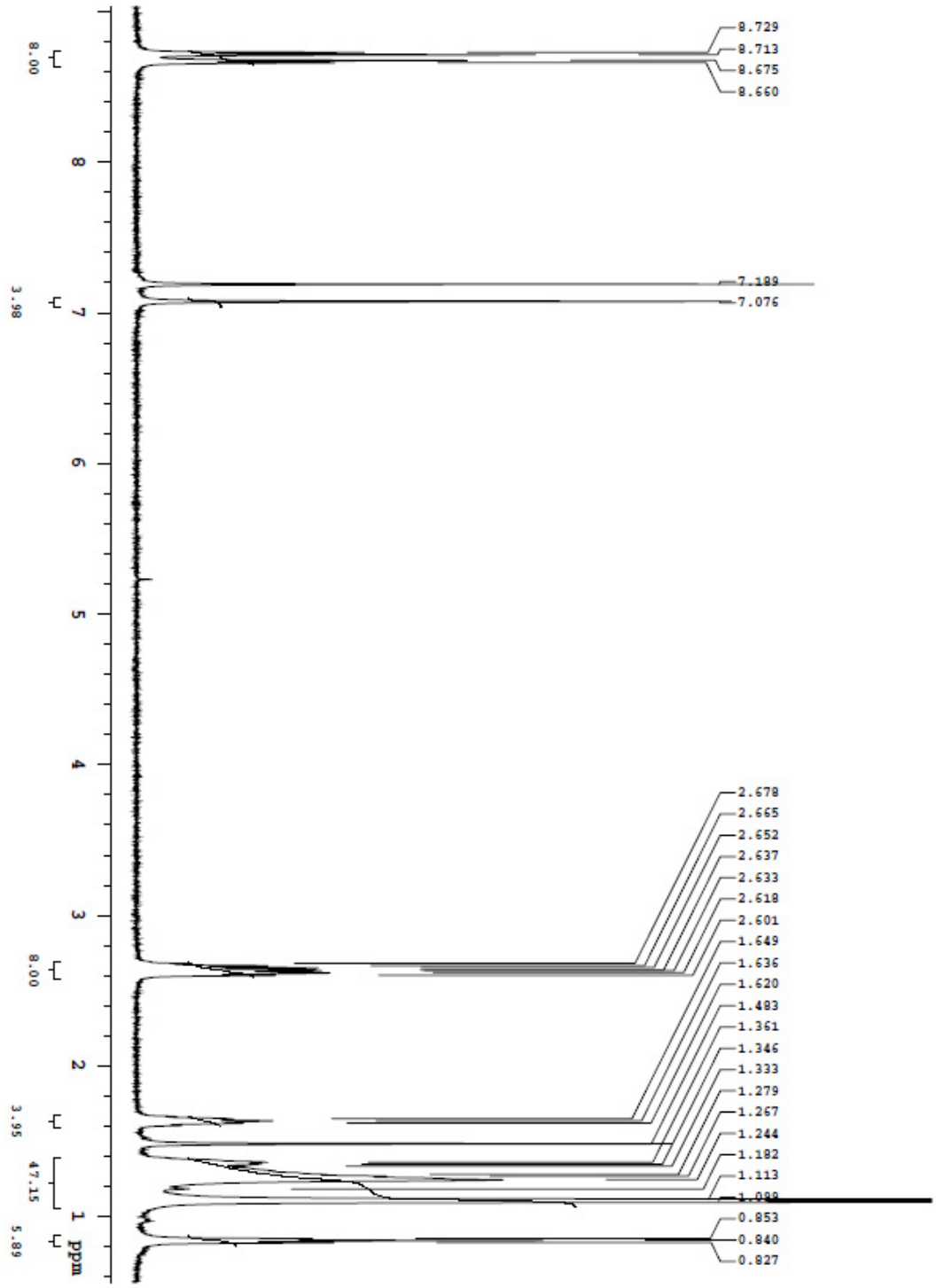

Figure S11. **7** ^{1}H NMR Spectrum in $CDCl_3$.

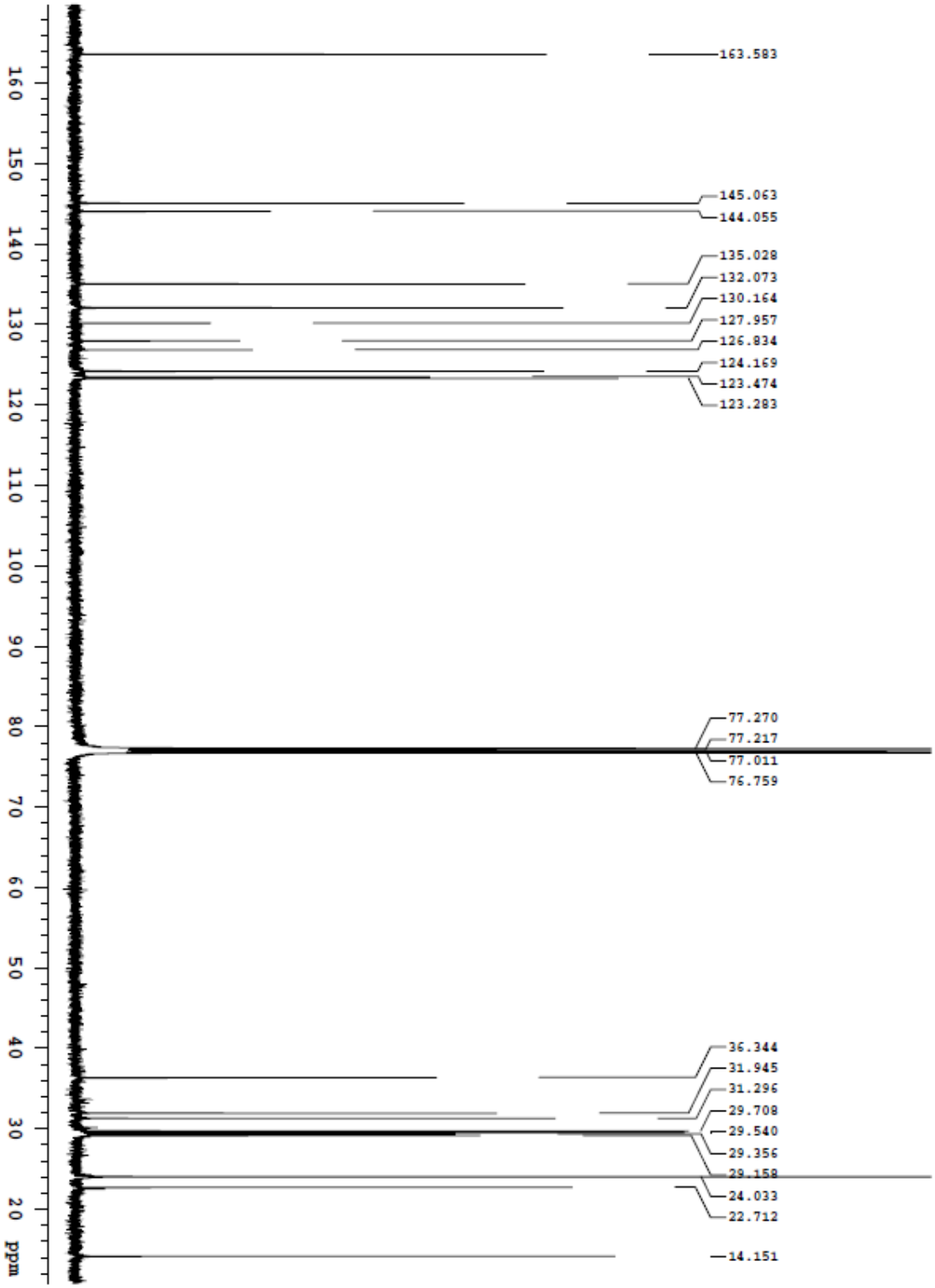

Figure S12. **7** ^{13}C NMR Spectrum in $CDCl_3$.

Absorption and Emission Spectra

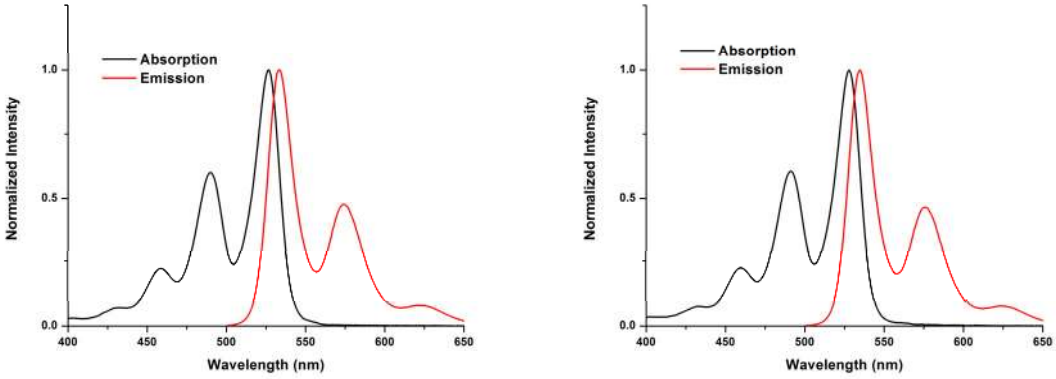

Figure S13. **1** (left) and **2** (right) normalized absorption and emission spectra in chloroform.

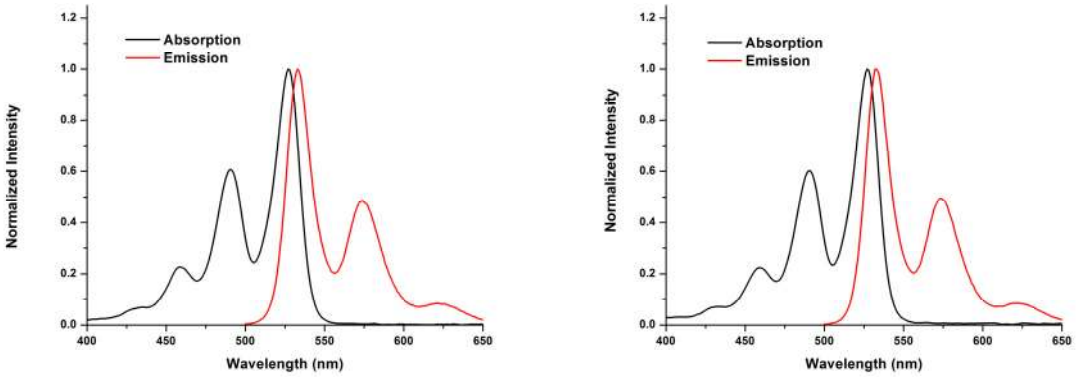

Figure S14. **3** (left) and **4** (right) normalized absorption and emission spectra in chloroform.

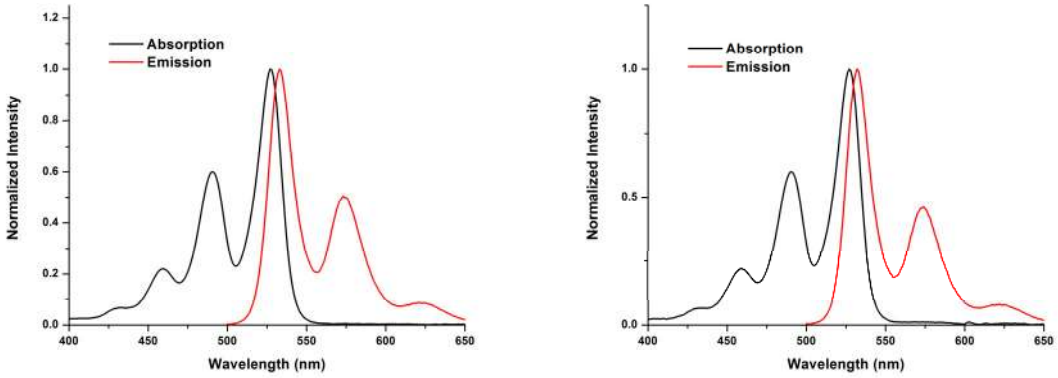

Figure S15. **5** (left) and **6** (right) normalized absorption and emission spectra in chloroform.

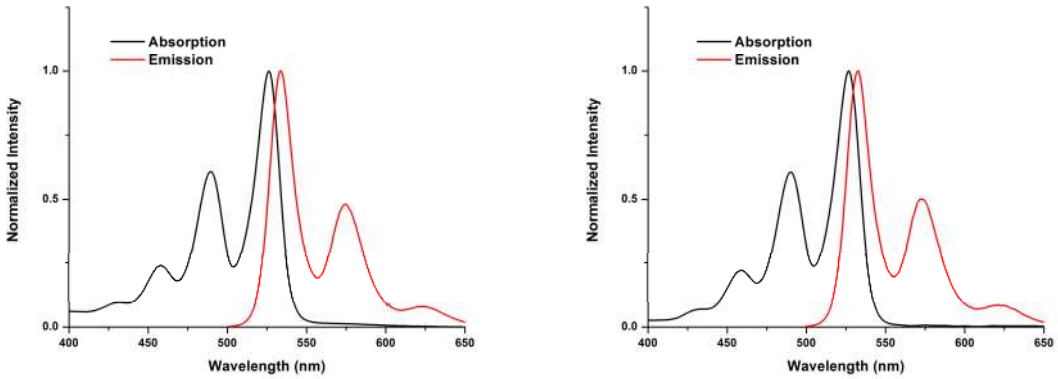

Figure S16. **7** (left) and **8** (right) normalized absorption and emission spectra in chloroform.

Molar Absorptivities

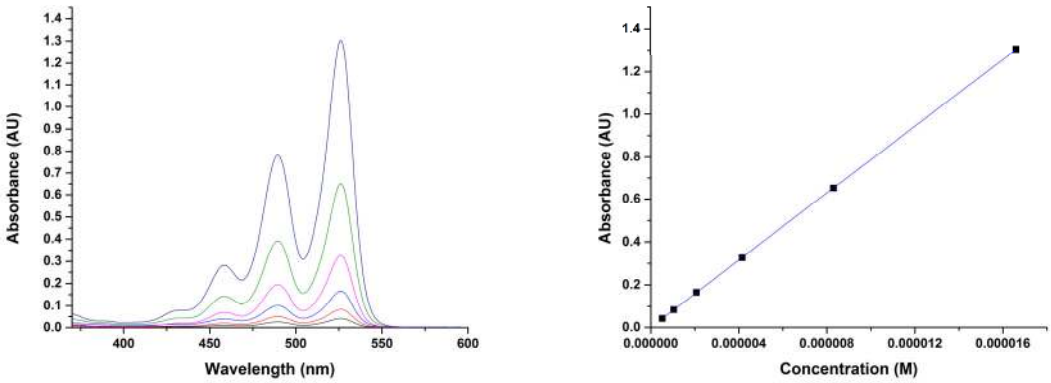

Figure S17. **1** Concentration dependent absorbance spectra ($CHCl_3$) and Beer's Law plot.

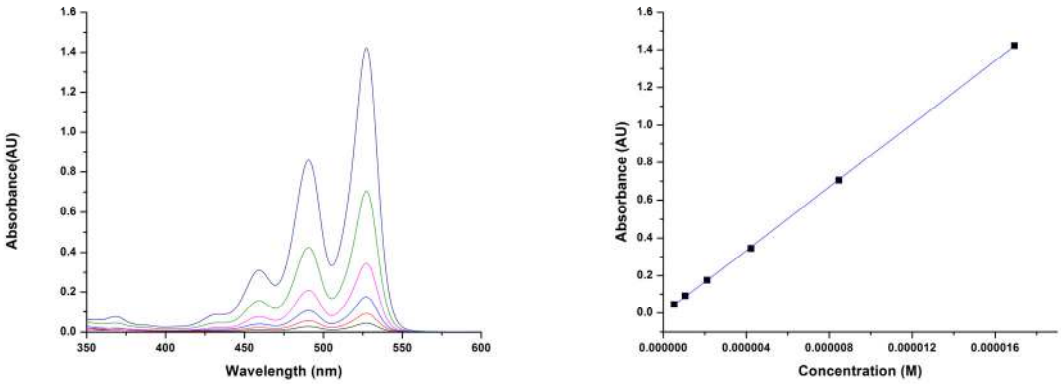

Figure S18. **2** Concentration dependent absorbance spectra ($CHCl_3$) and Beer's Law plot.

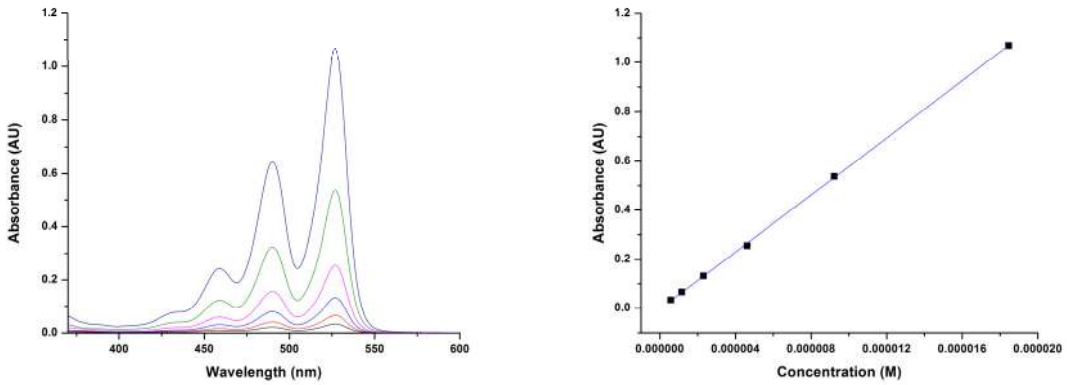

Figure S19. **7** Concentration dependent absorbance spectra ($CHCl_3$) and Beer's Law plot.

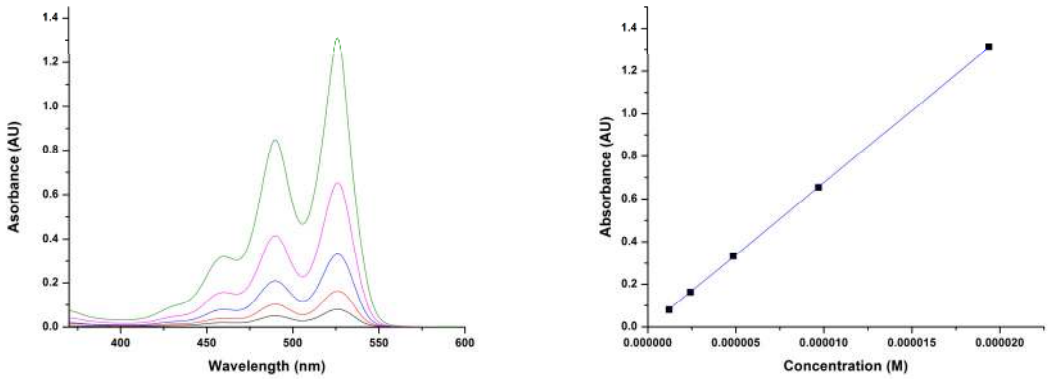

Figure S20. **4** Concentration dependent absorbance spectra and Beer's Law plot.

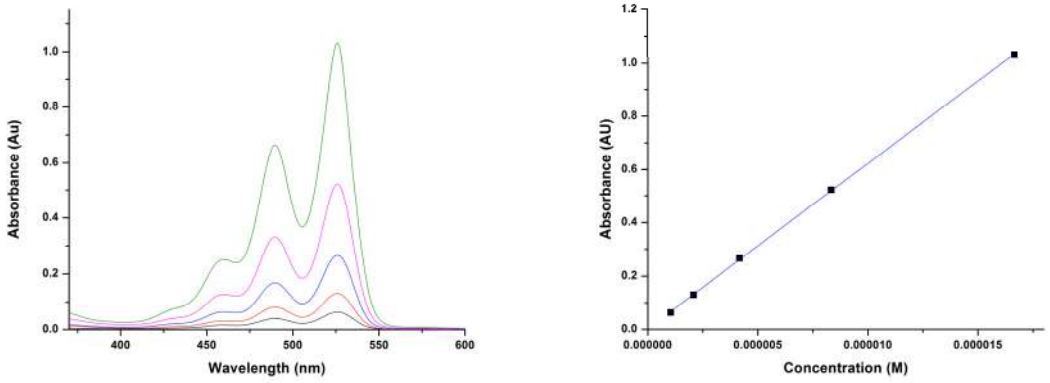

Figure S21. **6** Concentration dependent absorbance spectra and Beer's Law plot.

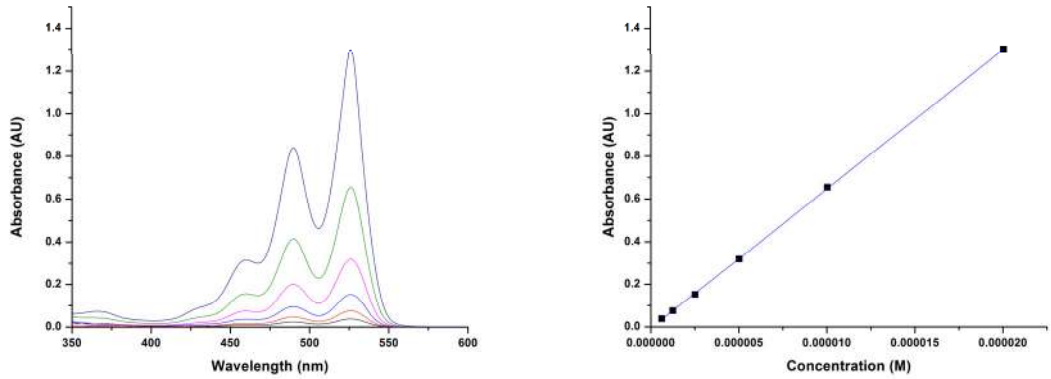

Figure S22. **5** Concentration dependent absorbance spectra and Beer's Law plot.

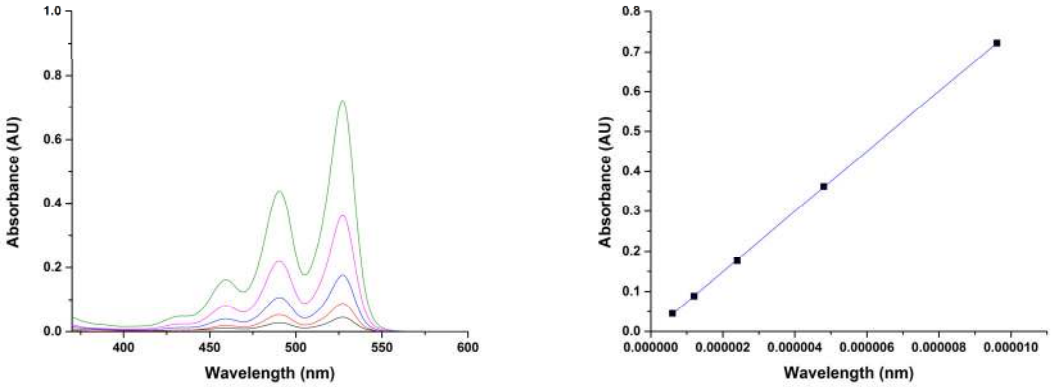

Figure S23. **3** Concentration dependent absorbance spectra and Beer's Law plot.

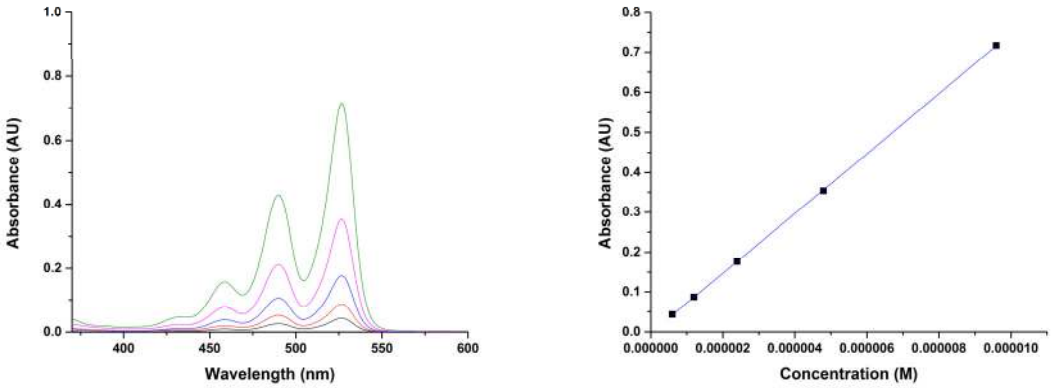

Figure S24. **8** Concentration dependent absorbance spectra and Beer's Law plot.

Table S1. λ_{abs}, λ_{em}, ε, and Φ values for fluorophores **1-8.**

Fluorophore	λ_{abs} (nm)	λ_{em} (nm)	ε	Φ
1	526	532	70350	.95
2	528	534	84500	.98
3	527	533	75300	.92
4	527	532	72450	.96
5	527	533	66800	.92
6	527	532	57900	.98
7	527	533	54950	.98
8	527	532	75000	.99

Order Parameters

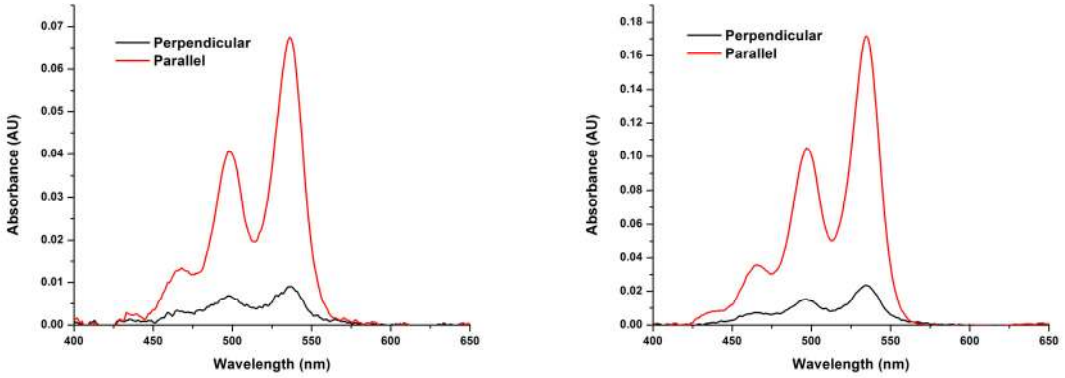

Figure S25. Polarized absorbance spectra measured parallel and perpendicular to the director **2** (left) and **3** (right) in planar photo-polymerized 5CB liquid crystal cells.

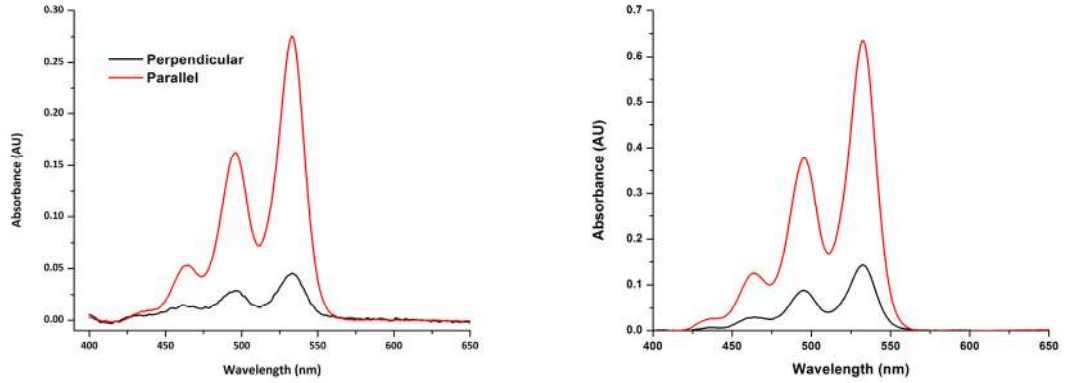

Figure S26. Polarized absorbance spectra measured parallel and perpendicular to the director **4** (left) and **5** (right) in planar photo-polymerized 5CB liquid crystal cells.

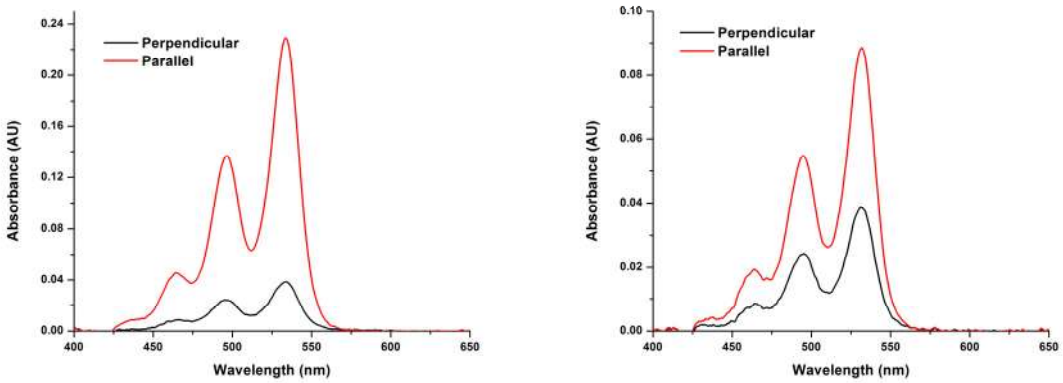

Figure S27. Polarized absorbance spectra measured parallel and perpendicular to the director **6** (left) and **7** (right) in planar photo-polymerized 5CB liquid crystal cells.

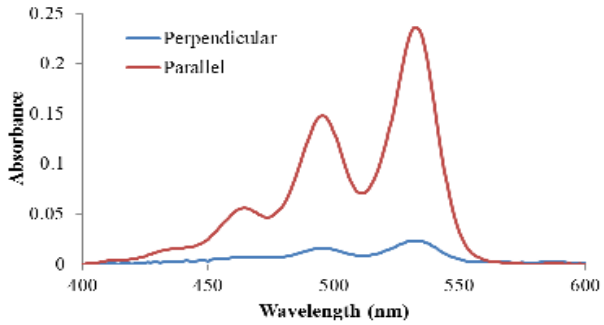

Figure S28. Polarized absorbance spectra measured parallel and perpendicular to the director for **4** in a planar photopolymerized RMM28A cell.